Syntheses, Structures and Electronic Properties of Zwitterionic Iron(II) and Cobalt(II) Complexes Featuring Ambidentate Tris(pyrazolyl)methanide Ligands

ARTICLE *in* CHEMISTRY - A EUROPEAN JOURNAL · MARCH 2009

Impact Factor: 5.73 · DOI: 10.1002/chem.200802317 · Source: PubMed

9 AUTHORS, INCLUDING:

Yanhua Lan
CNRS, Université Joseph Fourier et Grenobl…
159 PUBLICATIONS **3,367** CITATIONS
SEE PROFILE

Valeriu Mereacre
Karlsruhe Institute of Technology
139 PUBLICATIONS **2,415** CITATIONS
SEE PROFILE

Annie K. Powell
Karlsruhe Institute of Technology
488 PUBLICATIONS **12,217** CITATIONS
SEE PROFILE

CHEMISTRY
A EUROPEAN JOURNAL

DOI: 10.1002/chem.200802317

Syntheses, Structures and Electronic Properties of Zwitterionic Iron(II) and Cobalt(II) Complexes Featuring Ambidentate Tris(pyrazolyl)methanide Ligands

Istemi Kuzu,[a] Ivo Krummenacher,[a] Ian J. Hewitt,[a] Yanhua Lan,[a] Valeriu Mereacre,[a] Annie K. Powell,[a] Peter Höfer,[b] Jeffrey Harmer,[c] and Frank Breher*[a]

Abstract: By deprotonation of the corresponding tris(pyrazolyl)methane (^{Me}Tpm) precursor complexes [M(^{Me}Tpm)$_2$][(OTf)$_2$] (**1** and **2**), the zwitterionic tris(pyrazolyl)methanide iron(II) (**3**) and cobalt(II) (**4**) "sandwich" complexes of the general formula [M(^{Me}Tpmd)$_2$] are easily accessible. The structurally characterised complexes **3** and **4** are the first such homoleptic 3d transition metal species to feature two "naked", outward pointing pyramidal carbanions. Density functional theory calculations show metal-centred HOMOs and LUMOs with the destabilised carbanion orbitals in the energy region of the filled transition-metal-centred frontier orbitals. The electronic structures of these complexes have been investigated in detail by various spectroscopic techniques such as NMR, EPR, SQUID, Mössbauer, etc. Both complexes adopt a high-spin (HS) configuration at room temperature in solution and in the solid state. A thermally induced high-spin to low-spin (HS–LS) transition is observed for the iron(II) complex **3**. The HS–LS transition temperature of **3** in solution differs from that in the solid state, which in turn strongly depends on the amount of solvent molecules in the crystal lattice. Electrochemical studies on the corresponding cobalt(II) complex **4** provide evidence for a HS-Co^{II}⇌LS–Co^{III} transition upon oxidation, which was confirmed by preliminary synthetic oxidation reactions. Overall, it can be concluded that the related κ^3N-donor ligands tris(pyrazolyl)hydroborates (Tp^R) and ^{R}Tpmd ligands have similar bonding properties and that the metal cations experience more or less the same ligand environment.

Keywords: carbanions · electrochemistry · EPR spectroscopy · spin crossover · zwitterions

Introduction

There is a growing interest in versatile ligand systems[1] that can be regarded as monodentate and polydentate analogues of pentamethylcyclopentadienide (Cp^{*-}) and cyclopentadienide (Cp^-) anions. Although the differences in shape, energy and donor/acceptor properties of the frontier orbitals involved in metal bonding should not be neglected, several ligand systems and metal complexes of this type have been described in the literature. Selected examples are compiled in Scheme 1. The now familiar chemistry of metallacarboranes has its roots in the suggestion that the dicarbollide ligand, [η^5–7,8-*nido*-$C_2B_9H_{11}$]$^{2-}$ (**A**), and the corresponding carborane anions, are very similar to cyclopentadienide ligands.[2] The dicarbollide dianion has six delocalised electrons in pure π-type orbitals located on the open B_2C_3 pentagonal face.[3] Typical ligands featuring both σ- and π-donating properties include imides (**B**),[4] ketimides (**C**),[5] phosphorane iminates (**D**)[6] or the recently developed imidazolin-2-iminates (**E**),[7] which act as monodentate 2σ-4π-electron donors. Polydentate six-electron σ- and weakly π-donating ligands are exemplified by *fac*-coordinating κ^3N-donors such as tris(pyrazolyl)hydroborates (Tp^R, **F**)[8,9] and

[a] I. Kuzu, Dr. I. Krummenacher, Dr. I. J. Hewitt, Dr. Y. Lan, Dr. V. Mereacre, Prof. Dr. A. K. Powell, Prof. Dr. F. Breher
Institut für Anorganische Chemie
Universität Karlsruhe (TH)
Engesserstr. 15, 76131 Karlsruhe (Germany)
Fax: (+49) 721 608 70 21
E-mail: breher@aoc1.uni-karlsruhe.de

[b] Dr. P. Höfer
Bruker Biospin GmbH, EPR-Applikation
Silberstreifen, 76287 Rheinstetten (Germany)

[c] Dr. J. Harmer
Department of Chemistry
Centre for Advanced Electron Spin Resonance, University of Oxford
South Parks Road, Oxford OX1 3QR (UK)

Supporting information for this article is available on the WWW under http://dx.doi.org/10.1002/chem.200802317.

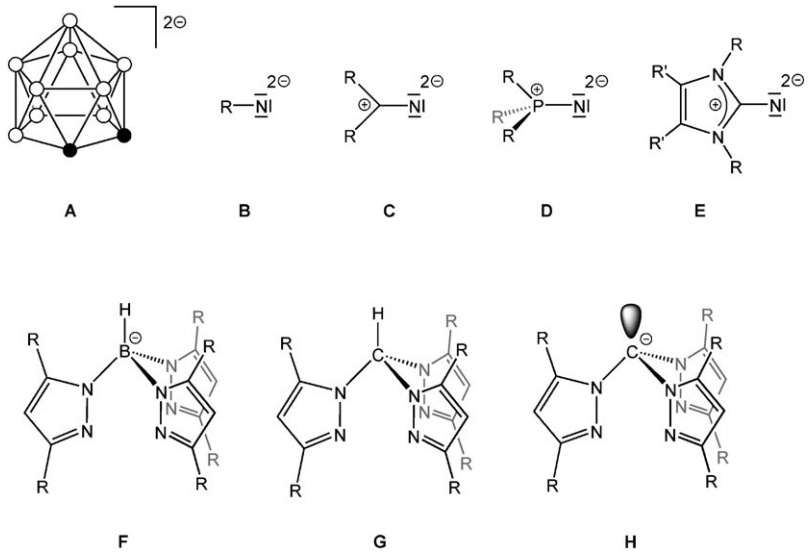

Scheme 1. Selected six-electron-donor ligands with intrinsically different donor properties.

their isoelectronic ($BH^- \leftrightarrow CH$), neutral tris(pyrazolyl)methane analogues ^{R}Tpm (**G**).[10]

Molecular "claw" ligands with a "podand topology",[11] such as tris(pyrazolyl)methanides $[C(R_2pz)_3]^-$ (^{R}Tpmd$^-$, **H**), are versatile ambidentate C^-/N_3 ligands which can act as κ^1C- or κ^3N-coordinating ligands, or both. Indeed, one particularly interesting aspect[12] of this class of anionic ligand system arises from the potentially reactive carbanion. The κ^1C-bonding mode of the carbanionic centre was first observed by Stone et al. in the early 1990's for the Au^I anion $[Au(^{Hr}Tpmd)C_6F_5]^-$.[13] In subsequent work, Mountford and Breher reported on the synthesis, structures and some computational studies of titanium(IV),[14] lithium,[15] copper(I), silver(I) and gold(I) complexes.[16] These collaborative studies on the chemistry of the ^{Me}Tpmd ligand were recently extended to the first sandwich and half-sandwich derivatives[17] of two representative divalent metals, namely Mg and Zn.[18]

Most of the aforementioned complexes are well-defined four- or six-coordinate monomeric zwitterions featuring κ^3N-coordinated ^{Me}Tpmd ligands with "naked", formally sp^3-hybridised, apical carbanions. So far, only the Au^I compounds have been shown to be coordinated by the apical carbanion of ^{R}Tpmd to form a linear, two-coordinate complex containing a covalent Au–C bond.[13,16] Since no homoleptic transition metal sandwich complex of the general formula $[M(^{R}Tpmd)_2]$ has been reported until now, it was of interest to check the accessibility, structure and electronic characteristics of such compounds and to compare them with the corresponding Tp^R or ^{R}Tpm complexes. Previously, we concluded that κ^3N-Tp^R and κ^3N-^{R}Tpmd have comparable bonding properties and that the metal atoms experience a similar ligand environment.[18] However, only the tris(pyrazolyl)methanides show ambidentate characteristics and dual functionality (κ^1C- *and* κ^3N-donor ligands).[1] Sandwich-type complexes are therefore of particular interest since the *two* outward pointing carbanionic centres are rigidly orientated to be diametrically opposed yet are still capable of acting as two electron κ^1C-donors, or so-called Janus ligands.[19] Multinuclear complexes should therefore be accessible upon subsequent κ^1C-coordination to secondary metal atoms (M′).

Results and Discussion

Herein we describe the syntheses, structures and detailed bulk and spectroscopic studies of the electronic properties of homoleptic, zwitterionic $[M(^{Me}Tpmd)_2]$ complexes. In addition, some density functional theory (DFT) studies have been used to support the findings of the presented experimental results.

Syntheses: In general, sandwich-type transition metal complexes of ^{R}Tpmd can be prepared by three different synthetic protocols. Equation (1) describes classical salt metathesis between the lithium reagent and metal halides. The second possibility [Eqn. (2)] is only applicable if a suitable transition metal precursor consisting of a base (B, for example, $[N(SiMe_3)_2]^-$) is available and depends strongly on the M–B bond strength within L_xMB_2. Alternatively, the zwitterionic $[M(^{R}Tpmd)_2]$ complexes can be prepared by pre-coordination of tris(pyrazolyl)methane (^{Me}Tpm) ligand to a divalent metal and subsequent deprotonation using suitable reagents such as sodium bis(trimethylsilyl)amide ($NaN(SiMe_3)_2$), lithium diisopropylamide (LDA) or lithium alkyls (RLi). It should also be noted that as a result of the zwitterionic nature of the divalent M^{II} complexes no counter-anions need to be involved, thus explaining the good solubility in non-polar solvents such as toluene.

$$2\,[Li(^{Me}Tpmd)(THF)] + MX_2 \rightarrow [M(^{Me}Tpmd)_2] + 2\,LiX \quad (1)$$

$$2\,^{Me}Tpm + L_xMB_2 \rightarrow [M(^{Me}Tpmd)_2] + 2\,BH + xL \quad (2)$$

$$[\{M(^{Me}Tpm)_2\}X_2] + 2\,M'B \rightarrow [M(^{Me}Tpmd)_2] + 2\,M'X + 2\,BH \quad (3)$$

The zwitterionic iron(II) (**3**) and cobalt(II) (**4**) complexes reported in this paper were synthesised according to Equation (3) by deprotonation of the corresponding bis-[tris(pyrazolyl)methane] complexes **1** and **2**, respectively. Thus, treatment of the dicationic precursors with two equivalents of sodium bis(trimethylsilyl)amide in THF directly afforded analytically pure, crystalline **3** and **4** in good yields (61%, **3**; 54%, **4**; Scheme 2) after standard workup procedures and recrystallisation from THF at 5 °C.

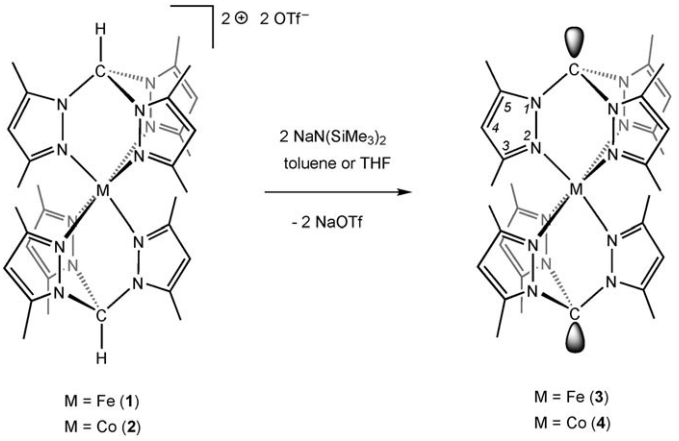

Scheme 2. Syntheses of **3** and **4**.

It is important to note that the dicationic precursor complexes $[M\{HC(3,5\text{-}Me_2pz)_3\}_2][(OTf)_2]$ (**1** and **2**; $OTf^- = [SO_3CF_3]^-$, triflate) must be prepared from the anhydrous salts $[Co(acn)_6][(OTf)_2]$ and $[Fe(OTf)_2(acn)_2]$ (acn = MeCN) and two equivalents of tris(3,5-dimethylpyrazolyl)methane in THF and must be thoroughly dried in vacuo. We found that the use of commercially available aqua complexes, $[M(H_2O)_6][(A)_2]$ ($A^- = [BF_4]^-$, $[PF_6]^-$), is unsatisfactory for this reaction as, although the products of the complexation reaction (i.e., **1** and **2**) were dried for several days at elevated temperatures and no trace of water was detectable by using NMR spectroscopy, these starting materials always led to undesirable side reactions and low yields of the targeted product.

The title compounds were isolated as colourless (**3**) or pale-yellow (**4**) crystalline solids, which are not very stable in air and are very moisture-sensitive, but thermally stable with decomposition points in excess of 200 °C. Their IR spectra (solid, attenuated total reflection, ATR) show the typical stretching frequencies of the pyrazole rings at around $\nu = 1548\ cm^{-1}$ for both complexes. In addition to the characteristic fragmentations, the EI mass spectra of **3** and **4** show the expected molecular ion envelope centred at m/z 650 (**3**) and 653 (**4**). The absence of higher mass peaks suggests that these compounds do not contain protonated ligands, in other words, ^{R}Tpm moieties. Crystals of the iron compound **3** obtained from THF contain two THF solvent molecules within the crystal lattice. These can be removed in vacuo, as shown by elemental analysis.

Before entering into further discussion of the spectroscopic findings in particular, it might be helpful to make some general comments and to summarise the results of some DFT calculations. Depending on the ligand-field strength of ^{Me}Tpmd in an octahedral field, **3** and **4** can generally adopt either a high-spin (HS) or a low-spin (LS) electron configuration (Scheme 3).[20] Standard UV/Vis spectroscopic studies in THF solution at room temperature, however, gave ambiguous data. A weak, broad and not well-defined absorption band was observed at around $\lambda = 550$ nm for the iron(II) complex **3**. Characteristic d-d transitions ($^5T_2 \rightarrow {}^5E$ in ideal octahedral symmetry) of comparable octahedral high-spin (HS) iron(II) complexes with *N*-donor ligands are found at around $\lambda = 800$ nm.[20] The UV/Vis spectrum of the analogous Co^{II} complex (**4**) in THF solution is comparable to that of **3** with more, albeit not well-defined, spectral features (see the Supporting Information).

As can be seen from the qualitative MO diagram calculated for the model compound $[Fe(^{Me}Tpmd)_2]$ (**Q3**, a D_{3d} symmetric model for the real compound **3**) in the high-spin (HS-**Q3**) and low-spin (LS-**Q3**) forms as two representative examples, these types of ^{Me}Tpmd transition metal complexes show metal-centred frontier orbitals ($27e_g$ and $28e_g$ in Scheme 3). The same qualitative ordering of the orbitals was

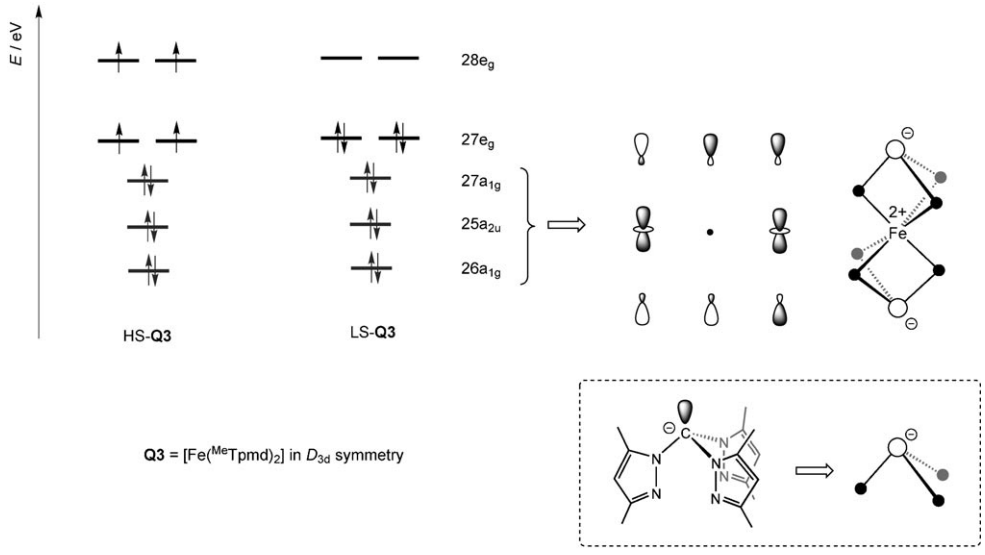

Scheme 3. Qualitative molecular orbital (MO) diagram for high-spin (HS) and low-spin (LS) $[Fe(^{Me}Tpmd)_2]$ (**Q3**) and schematic drawings of selected MOs (TURBOMOLE, RI-DFT, BP86, def2-TZVP, D_{3d} symmetry).

found for the analogous Tp complexes.[21] However, DFT calculations of the zwitterionic magnesium and zinc complexes [M(^{Me}Tpmd)$_2$] (M = Mg, Zn), as well as the titanium(IV),[14] lithium,[15] copper(I) and silver(I)[16] complexes containing a κ^3N-coordinated ^{Me}Tpmd ligand, have shown that the HOMO for these complexes is a ^{Me}Tpmd-based carbanion lone-pair. DFT studies have also shown that the pyrazolyl ring substituents destabilise the carbanion lone-pair and that the nature of the metal ion has little influence.[18] Therefore, an important point in the organometallic and coordination chemistry of the ambidentate ^{R}Tpmd ligand is the energetically destabilised carbanion orbital, which is not present in either Tp^R or ^{R}Tpm ligands. Even if the ^{R}Tpmd ligand is compared with analogous *N*- or *P*-based ligand systems (N(pz)$_3$/P(pz)$_3$ vs. [C(pz)$_3$]$^-$),[1,22] only the carbanion donor orbital can be found in the energy region of the filled, transition-metal-centred frontier orbitals,[23] here either Fe (**3**) or Co (**4**). As a result of this, symmetry-allowed mixing of one transition metal orbital (d_{z^2}-type) and the carbanion-centred orbitals can be observed ($27a_{1g}$, $26a_{1g}$ and $25a_{2u}$ in Scheme 3).

NMR spectroscopy: The first indications for the spin preference (paramagnetic HS vs. diamagnetic LS) of **3** in solution were provided by ^{1}H NMR spectroscopic studies—the broad signals and chemical shifts of the proton resonances in the ^{1}H NMR spectrum of **3** in [D$_8$]THF at room temperature clearly indicated the presence of unpaired electrons (Figure 1). We have also frequently observed low-intensity signals, owing to a by-product formed by partial oxidation of **3**. The redox behaviour of **3** will be discussed below.

In light of the large chemical shifts at room temperature characteristic of paramagnetic complexes, the above-mentioned high-spin configuration (HS-**3**; $(27a_{1g})^2$, $(27e_g)^2$, $(28e_g)^2$ in D_{3d} symmetry) was anticipated for **3**. No diamagnetic resonances, apart from those arising from residual solvent protons, were detected. The ^{1}H NMR spectrum of **3** in [D$_8$]THF at 296 K exhibits three broad but well-defined resonances at $\delta = 50.0$ (4-CH$_{pz}$), 39.4 (3-CH$_3$) and 13.5 ppm (5-CH$_3$). These signal assignments were made on the basis of the corresponding relative integration and the expected single set of signals for a symmetrical complex. In light of the line width, and taking the distance between the iron centre and the protons into account, the individual methyl groups in the 3- and the 5-positions of the pyrazolyl ring can also be assigned within a certain probability (the line width, $\Delta\nu$, of a paramagnetic resonance signal increases with decreasing distance from the corresponding dipoles). Lowering the temperature by a few degrees leads to non-linear changes in the chemical shifts. As can be seen from the temperature-dependent (296–183 K) ^{1}H NMR spectra of **3** shown in Figure 1, the temperature-dependence of the isotropic shifts does not follow the Curie law (or extended Curie law to account for thermally accessible excited states; see also Figure S6 in the Supporting Information).[24] Between 296 and 253 K the changes are relatively small ($\Delta\delta$(CH$_{pz}$) = 7.2 ppm; $\Delta\delta$(CH$_3$) = 8.3 and 0.5 ppm), although below this temperature we observed a behaviour indicative of a fast thermally induced high-spin/low-spin (HS–LS) equilibrium.[25] All resonances are considerably broadened at $T < 253$ K and coalesce into one signal centred at $\delta =$ 11.1 ppm (183 K). The observation of a single set of resonances in the ^{1}H NMR spectra indicates that the attainment of the HS–LS equilibrium is fast on the NMR time scale. We did not detect individual sets of resonances for either the diamagnetic low-spin complex (LS-**3**; $(27a_{1g})^2$, $(27e_g)^4$) or the paramagnetic high-spin complex HS-**3**. A similar rapid exchange has been observed previously by Trofimenko et al. for the complex [Fe{HB(pz)$_3$}$_2$],[26] whereas two distinct sets of resonances were observed by Reger and Long for [Fe{HC(pz)$_3$}$_2$][(BF$_4$)$_2$] in DMF solutions at temperatures below 283 K (slow exchange on the NMR time scale).[27] Based on our data we would estimate a HS–LS transition temperature ($\gamma_{HS}/\gamma_{LS} = 1$) of around 213 K in solution, with an onset of the transition at around 253 K. Studies performed in the solid state are discussed in detail below. In [D$_8$]THF, however, we were not able to shift the HS–LS equilibrium by lowering the temperature to an appropriate extent to detect pure LS-**3** in solution.

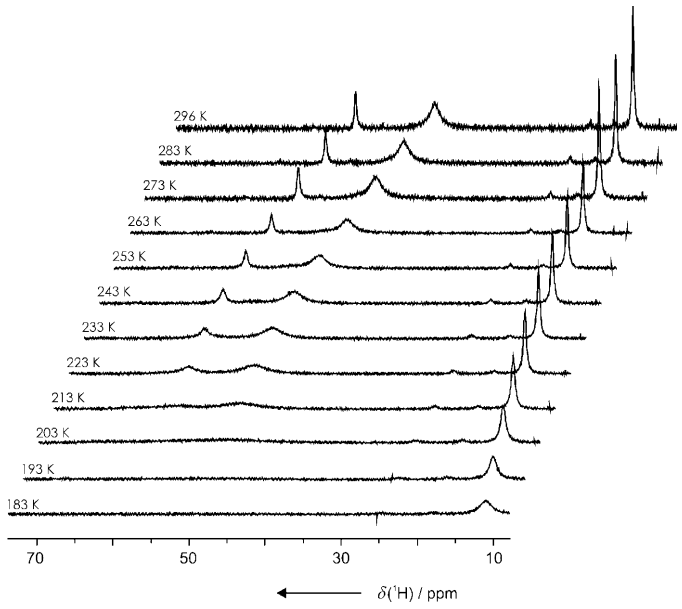

Figure 1. Temperature-dependent (296–183 K) ^{1}H NMR spectra for **3** ([D$_8$]THF).

Similar ^{1}H NMR spectra were recorded for the corresponding cobalt(II) complex **4** (Figure 2) despite the fact that this complex should be paramagnetic in both the high-spin (HS-**4**; $(27a_{1g})^2$, $(27e_g)^3$, $(28e_g)^2$) and low-spin (LS-**4**; $(27a_{1g})^2$, $(27e_g)^4$, $(28e_g)^1$) states.[28] Again, broad but well-defined signals, with chemical shifts of $\delta = 52.2$ (CH$_{pz}$), 50.2 (CH$_3$), and −87.2 ppm (CH$_3$), were observed for the protons in the ^{1}H NMR spectrum of **4** at 296 K. These values differ significantly from those of **3**. Decreasing the temperature led to large changes in the positions of the resonances (see also Figure S7 in the Supporting Information).

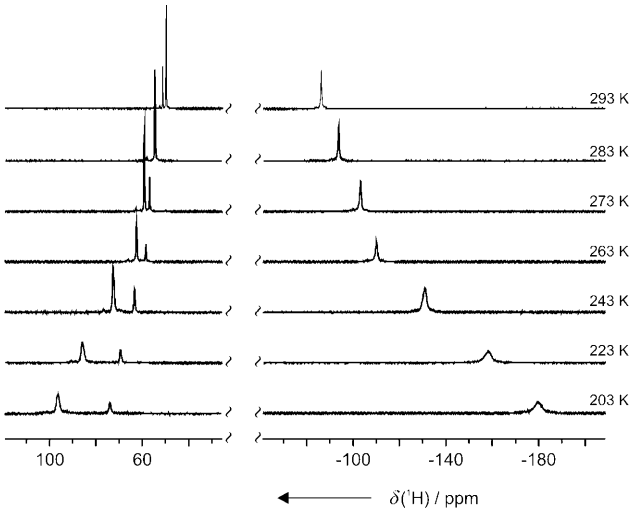

Figure 2. Temperature-dependent (296–203 K) ^{1}H NMR spectra for **4** ([D$_8$]THF). The diamagnetic region of the spectrum, which shows only residual solvent peaks and small amounts of impurities, has been omitted for clarity.

Upon cooling, the chemical shift difference for the methyl protons becomes very large ($|\Delta\delta_{3,5}| \approx 280$ ppm at 203 K).[29] At first sight, these changes are consistent with the Curie law behaviour expected for a paramagnetic complex,[30] but closer inspection reveals some deviation from the ideal Curie law straight line. The intercepts differ significantly from zero if simple Curie behaviour is assumed by plotting straight lines in a δ vs. $1000/T$ diagram (Figure S7 in the Supporting Information). Possible reasons for this could be thermally accessible excited states or large dipolar shifts owing to the large magnetic anisotropy (zero-field splitting) of the cobalt centre. We have tried to analyse the curvature of the temperature-dependence of the isotropic shift by using the TDF program written, and originally developed, by Shokhirev and Walker for iron porphyrins.[31] However, although the initial fit looked promising (Figure S8 in the Supporting Information), the fitting parameters obtained by the implemented optimisation routine were not reasonable. Furthermore, attempts to apply the complementary Evans method to determine the magnetic susceptibility in solution failed to give unambiguous data.

Magnetic, Mössbauer, and EPR investigations: In view of the paramagnetic nature of **4** and a conceivable thermally induced HS–LS transition for **3**, we performed some magnetic and Mössbauer studies as well as EPR investigations. Figure 3 shows the magnetic susceptibilities in the form of a χT vs. T plot for the iron complex **3**, from which the anticipated temperature-dependence of the spin state is immediately apparent. Complex **3** is a "classical" example of an iron(II) spin-state crossover that can be induced in a high-spin complex upon cooling.[20,32] It is important to note that these SQUID studies were performed with thoroughly dried samples of **3**, which in turn did not contain any THF solvent molecules (for conclusions from X-ray studies on **3**·2THF see below).

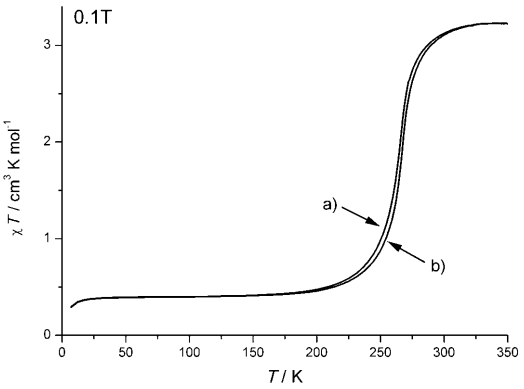

Figure 3. Magnetic susceptibilities of thoroughly dried and lattice-solvent-free samples of **3** plotted as χT vs. temperature. The data obtained upon initial cooling from 350 to 7 K are indicated by curve a) and those for the re-heating process are indicated by curve b)

Above 300 K, χT is almost temperature-independent, with a value of 3.22 cm^3 K mol^{-1} ($\mu_{eff} = 5.07\ \mu_B$), which is very close to the value of around 5.2 μ_B often observed for high-spin iron(II) complexes. The spin-only magnetic moment would be 4.90 μ_B. A transition from high-spin iron(II) (HS-**3**), with a nominal $(27a_{1g})^2$, $(27e_g)^2$, $(28e_g)^2$ electronic configuration in D_{3d} symmetry ($S=2$), occurs gradually from about 300 K but then relatively abruptly leads to LS-**3** with a singlet ground state ($S=0$, $(27a_{1g})^2$, $(27e_g)^4$). The HS–LS transition is centred at around 267 K, which is approximately 50 K higher than the estimated value in solution. Between 7 and approximately 200 K, χT is not zero and increases slightly from a χT value of about 0.30 cm^3 K mol^{-1} ($\mu_{eff} = 1.55\ \mu_B$) at 7 K. This non-zero moment is a consequence of the second-order Zeeman mixing of magnetic excited-state wave functions with the non-magnetic ground-state wave function (temperature-independent paramagnetic contribution to the magnetic moment). However, it is slightly larger than usually observed in similar systems but fairly typical of low-spin iron(II) complexes. The χT value most probably indicates the presence of small amounts of partially oxidised, paramagnetic by-products, which were also seen in the NMR studies (see above). The data were recorded using both zero-field cooling and warming modes to detect possible hysteresis effects. Only a small hysteresis could be observed upon re-heating the sample (Figure 3b).

The results of the bulk susceptibility studies are supported by Mössbauer measurements, which were also performed on solvent-free samples of **3** (Figure S2 in the Supporting Information). The expected small amounts of by-products resulting from the sensitivity of **3** to air (oxidation) and moisture (protonation) were observed, and for this reason we do not propose to give exact HS–LS fractions. Nevertheless, Mössbauer spectroscopy shows conclusively that the complex transforms almost completely from HS-**3** to LS-**3** between 300 and 100 K. The 300 K spectrum shows a large quadrupole splitting ($\Delta E_Q = 3.59$ mm s^{-1}) and an isomer shift, δ, of 1.02 mm s^{-1} (relative to α-iron foil at room temperature) and is similar to that observed in [Fe{HB(3,5-Me$_2$pz)$_3$}$_2$] ($\delta =$

1.03 mm s^{-1}; $\Delta E_Q = 3.67$ mm s^{-1}) and many other octahedrally coordinated HS-Fe^{II} complexes featuring *N*-donor ligands.[33] There is also some LS-Fe^{II} present, which at this temperature does not crossover to the HS state. Full transformation to HS-Fe^{II} is expected at temperatures close to 350 K, although 300 K is the limit of the measurements we are able to perform with our Mössbauer spectrometer. A good fit of the 300 K spectrum was obtained by taking into consideration the presence of a small amount of oxidised product. At low temperatures, the doublets of the HS component are significantly diminished and a narrow doublet at $\delta = 0.50$ mm s^{-1} and $\Delta E_Q = 0.20$ mm s^{-1}, characteristic of a LS-Fe^{II} complex, increases in intensity. This doublet has a small quadrupole splitting because the electric field gradient at the Fe nucleus for LS-**3** and is a result of the lattice charge distribution. The electronic contribution to the electric field gradient for LS-Fe^{II} is zero.

Although it is already well-known that small effects in the solid-state can considerably influence the HS–LS behaviour for a given compound,[34] it was of interest to compare the HS–LS transition temperature for **3** with those known for Tp^R and ^{R}Tpm complexes of iron(II). Selected examples from a compilation published recently by Reger and Long[35] are shown in Table 1. The directly related zwitterionic tris-

Table 1. Thermally induced HS–LS transition temperatures of related iron(II) complexes.

Tp^R complexes	^{R}Tpm complexes
[Fe{HB(3,5-Me$_2$pz)$_3$}$_2$]	[Fe{HC(3,5-Me$_2$pz)$_3$}$_3$][(BF$_4$)$_2$]
190 K	190 K (partial transition)
[Fe{HB(3,4,5-Me$_3$pz)$_3$}$_2$]	[Fe{HC(3,4,5-Me$_2$pz)$_3$}$_2$][(BF$_4$)$_2$]
$<$4 K	110 K
[Fe{HB(pz)$_3$}$_2$]	[Fe{HC(pz)$_3$}$_2$][(BF$_4$)$_2$]
$\approx$335 K	$>$300 K (HS at 472 K)[a]

[a] As indicated by Mössbauer data.

(pyrazolyl)hydroborate complex [Fe{HB(3,5-Me$_2$pz)$_3$}$_2$] shows a transition temperature of around 190 K, which is considerably lower than the value obtained for **3** (267 K).

In contrast to **3**, the cobalt compound **4** is a high-spin complex at all temperatures studied by SQUID measurements (1.8–300 K; Figure S5 in the Supporting Information). At room temperature, the product χT is 3.09 cm^3 K mol^{-1} ($\mu_{eff} = 5.0$ μ_B), which falls in the typical region for octahedrally coordinated high-spin Co^{II} compounds ($S = 3/2$, approx. 4.7–5.2 μ_B).[36] Upon cooling the polycrystalline sample, the χT product drops continuously to reach a value of 1.57 cm^3 K mol^{-1} at 5 K. The χT product increases slightly below 5 K at an applied magnetic field of 1000 Oe, which might be due to either a significant anisotropy or weak antiferromagnetic interactions between the complexes. We observed a considerable decrease of χT with an applied field of 10000 Oe at temperatures below 5 K, presumably due to the onset of saturation of the magnetisation. It did not prove possible to simulate these data satisfactorily.[37]

Solutions of the iron complex (**3**) in toluene are EPR-silent at room temperature. This is due to spin-orbit coupling within the high-spin state for iron(II), which leads to spin-lattice relaxation times so short that EPR spectra can only be observed at very low temperatures.[38] Owing to the HS–LS transition mentioned above, the sample is, as expected, EPR-silent at low temperatures. Toluene solutions of the cobalt analogue **4** also showed no EPR signal at room temperature. This can again be attributed to the spin-orbit coupling in the HS state, which decreases the spin-lattice relaxation times and makes recording signals at around room temperature difficult. However, as expected, samples of **4** show strong signals upon cooling to 20 K. Figure 4 summarises the

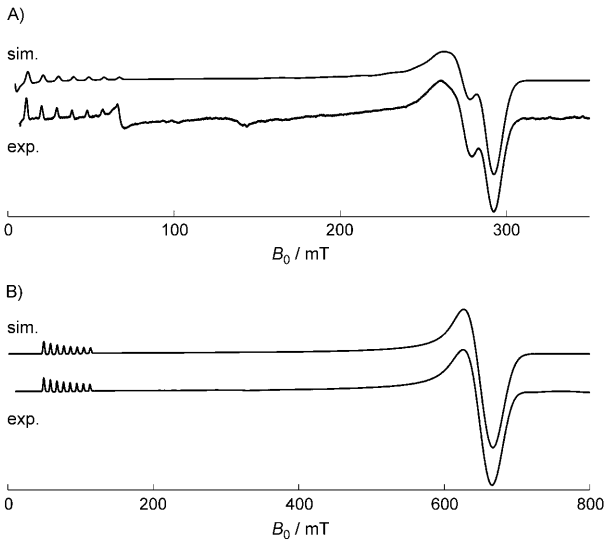

Figure 4. Experimental (exp.) and simulated (sim.) continuous wave (CW) EPR spectra of **4** in toluene solution at 20 K at A) S-band and the B) X-band.

continuous wave (CW) EPR spectra of **4** in toluene recorded at S-band (top) and X-band (bottom), along with the corresponding simulations for a system with an effective electron spin, S', of $^1/_2$. The spin-Hamiltonian parameters used for the simulations are: $g_{\perp 1} = 1.02$, $g_{\perp 2} = 1.08$ and $g_{\parallel} = 8.20$, with a hyperfine coupling to the Co^{2+} ion ($I = ^7/_2$) of $A_{\perp 1} = 50$, $A_{\perp 2} = 50$ and $A_{\parallel} = 1050$ MHz. Comparable values can be found in the literature for sandwich-type cobalt(II) Tpm and Tp complexes.[39,40] An effective electron spin of $^1/_2$ is appropriate in this case as the zero-field splitting (ZFS) is much larger than the microwave frequency ($<$10 GHz) and thus EPR transitions are only observed within the lowest Kramers doublet. An estimation of the ZFS was obtained from relaxation measurements. Orbach and co-workers have shown that the temperature-dependence of the spin-lattice relaxation rate for a Kramers ion directly yields an estimate of the ZFS energy $2|D|$.[41] By the Orbach mechanism, electron spin-lattice relaxation occurs by a spin-flip transition coupled to phonon absorption or emission, which connects the ground state to a low-lying excited state. This relaxation mechanism dominates in a temperature range intermediate

between the direct and Raman regions. The relaxation rate resulting from the Orbach mechanism can be defined according to Equation (4),

$$\frac{1}{T_1} = \frac{A}{e^{\Delta/kT}-1} \cong A\, e^{-\Delta/kT} \qquad (4)$$

in which T_1 is the spin-lattice relaxation, k is the Boltzmann constant, A is a coefficient characteristic of the phonon-spin coupling properties of the matrix, and Δ is the energy gap between the ground and lowest lying excited state. When the low-lying excited state is the next highest Kramers doublet of the $S = {}^3/_2$ Co^{2+} ion, and $\Delta < k\theta$, in which θ is the Debye temperature, a plot of $\ln(T_1)$ vs. $1/T$ will yield an estimate of Δ (approx. $2|D|$).[42]

Figure 5 shows a plot of $\ln(T_1)$ vs. $1/T$ in the temperature range 6–15 K with the rates $1/T_1$ being measured at $g_\perp$ using a pulse saturation recovery sequence (see the Experimental Section). The splitting between the two lowest Kramers doublets of the high-spin Co^{2+} ion was estimated from the slope of the linear region of the plot between 10 and 15 K ($\Delta =$ 40 cm^{-1}; $\approx 2|D|$).[40,43] The curvature below this temperature range indicates the onset of spin-lattice relaxation by the direct process.[38]

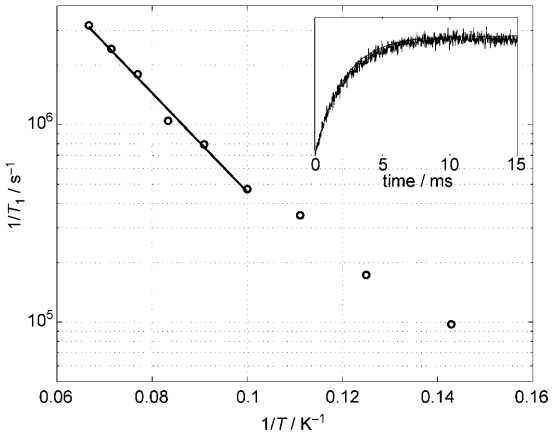

Figure 5. Plot of $\ln(T_1)$ vs. $1/T$ in the temperature range 6–15 K; Inset: recovery curve which was monitored by the primary echo sequence using mw pulses. The observer position corresponds to $g_\perp$.

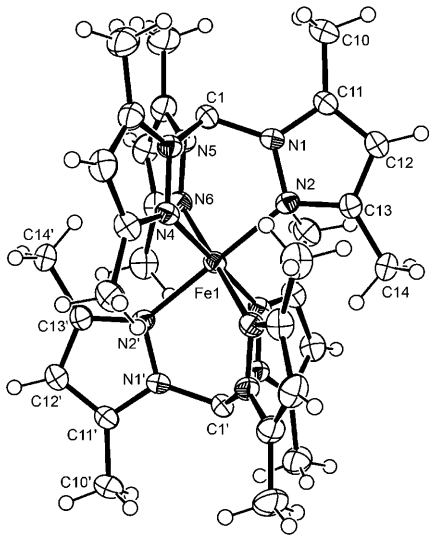

Figure 6. Molecular structure of [Fe(^{Me}Tpmd)$_2$] (**3**·2THF) at 178 K; displacement ellipsoids are drawn at the 50% probability level. Equivalent atoms denoted with a prime are generated by $-x+1$, $-y+1$, $-z+1$.

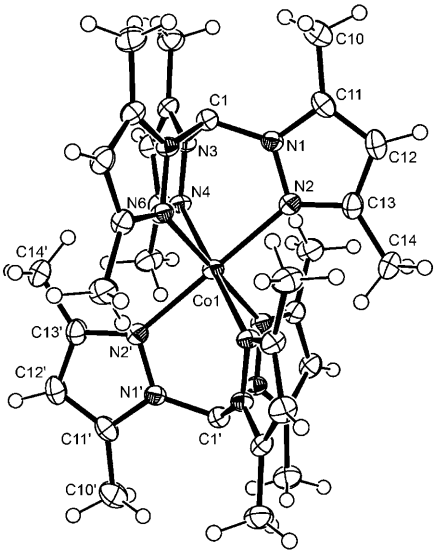

Figure 7. Molecular structure of [Co(^{Me}Tpmd)$_2$] (**4**); displacement ellipsoids are drawn at the 50% probability level. Equivalent atoms denoted with a prime are generated by $-x+1$, $-y+1$, $-z+1$.

Molecular structures: The crystal-structure determination of **3**·2THF (Figure 6) and **4** (Figure 7) verified the formation of zwitterionic iron(II) and cobalt(II) complexes in which the metal cations are coordinated by six pyrazole nitrogen atoms. As expected, the formally sp^3-hybridised carbanions (C1 and C1′) are oriented in opposite directions. Both complexes crystallise in the triclinic space group $P\bar{1}$ with the metal atoms on an inversion centre ($Z = 1$) and with **3** crystallising along with two THF solvent molecules in the lattice, as mentioned above. Selected bond lengths and angles for both complexes are compiled in Table 2.

The six nitrogen atoms in **4** span a trigonally distorted octahedron (approximately D_{3d} symmetry) around the Co atom. Accordingly, two principal ranges of N–Co–N angles were detected (84.6–86.0° and 94.0–95.4°). The average cobalt–nitrogen distance (217.8(3) pm) compares well with those reported for high-spin cobalt(II) complexes.[44]

To elucidate the structural changes caused by the HS to LS transition of the corresponding iron(II) complex **3**·2THF, full X-ray structure analyses on one single crystal were determined at two different temperatures (178 and 278 K). No phase transition occurred upon cooling. However, the unit cell data compiled in Table 3 strongly support

Table 2. Selected bond lengths [pm] and angles [°] for **4** (M1 = Co1), HS-**3**·2THF and LS-**3**·2THF (M1 = Fe1).[a]

	4	HS-**3**×2 THF	LS-**3**×2 THF
C1–N1	144.7(4)	144.3(3)	144.6(3)
C1–N3	143.8(4)	143.7(4)	144.6(3)
C1–N5	144.3(4)	143.7(4)	144.4(3)
M1–N2	214.8(3)	217.1(2)	199.1(2)
M1–N4	211.8(2)	215.0(2)	198.2(2)
M1–N6	212.9(2)	217.9(2)	199.5(2)
C1···M1	317.4	319.0	307.3
N2–M1–N4	84.87(9)	84.52(8)	88.11(9)
N2–M1–N6	86.0(1)	85.49(8)	88.56(9)
N4–M1–N6	84.56(9)	83.78(9)	87.60(9)
N2–M1–N4′	95.13(9)	95.48(8)	91.89(9)
N2–M1–N6′	94.0(1)	94.51(8)	91.44(9)
N4–M1–N6′	95.4(1)	96.22(9)	92.40(9)
N1–C1–N3	109.1(2)	109.5(2)	108.0(2)
N1–C1–N5	108.2(2)	108.2(2)	106.5(2)
N3–C1–N5	108.8(2)	109.5(2)	107.4(2)

[a] Equivalent atoms denoted with a prime are generated by $-x+1$, $-y+1$, $-z+1$.

Table 3. Temperature-dependent unit cell parameters for **3**·2THF

Temperature	**178 K**	**278 K**
a [pm]	875.7(2)	866.7(2)
b [pm]	967.4(2)	991.1(2)
c [pm]	1327.9(3)	1357.5(3)
α [°]	109.62(3)	109.11(3)
β [°]	98.66(3)	98.39(3)
γ [°]	100.81(3)	99.81(3)
V [$\times 10^6$ pm^3]	1012.7(4)	1059.8(4)

a considerable shrinking of the cell volume upon cooling (from $1059.8(5)\times10^6$ pm^3 at 278 K to $1012.7(5)\times10^6$ pm^3 at 178 K), which cannot be a pure effect of temperature on the unit cell parameters. This shrinking of the cell volume is accompanied by a colour change of the single crystal mounted on the goniometer from colourless to deep purple. The thermal HS to LS transition is clearly evident from the change in the average iron–nitrogen distances ($|\Delta d| = 17.8$ pm; average d_{HS}(Fe–N) = 216.7(2) pm; d_{LS}(Fe–N) = 198.9 pm), with much smaller values for LS-**3**·2THF. Comparable values have been reported for both HS and LS complexes of iron(II).[35] As with the corresponding cobalt complex, the coordination sphere around Fe^{II} at both temperatures and, hence, both spin states, is trigonally distorted, although the distortion is much more pronounced for HS-**3** (average N–Fe–N angles: 88.09° and 91.91° (LS); 84.60° and 95.40° (HS)). As a consequence of the shorter iron–nitrogen distances and much less trigonally distorted octahedral geometry, the C1···Fe1 distances are smaller for the low-spin complex (d_{LS}(C1···Fe1) = 307.3 pm vs. d_{HS}(C1···Fe1) = 319.0 pm).

As may be envisaged from the overlaid structures in Figure 8, the Fe–N bond-lengthening corresponds, at first glance, to a kind of symmetrical "breathing". As the M–N distance increases, the ligand opens up and the bite-size increases.[45] Seemingly, the anionic, κ^3N-coordinating ligand ^{Me}Tpmd can comfortably accommodate a variety of metal

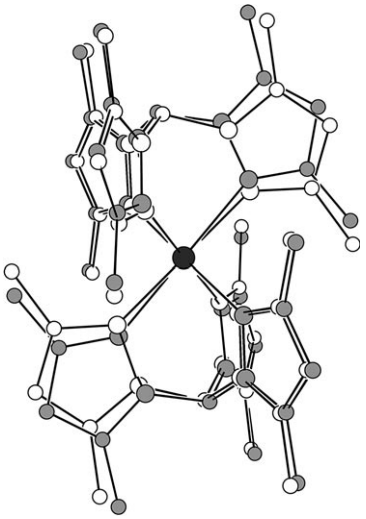

Figure 8. Comparison of the X-ray structure analyses of HS (grey) and LS (white) iron(II) complex **3** measured at 278 and 178 K, respectively (iron in dark grey). The atoms were drawn with equivalent, but arbitrary radii.

sizes by opening up, comparable to the conformational flexibility of tridentate scorpionate ligands recently discussed by Zimmer et al.[46]

All structural parameters for both the HS and the LS complex were confirmed by quantum chemical calculations using the TURBOMOLE program and density functional methods (RI-DFT, BP86, def2-TZVP) for the model compound **Q3** in D_{3d} symmetry (see the Experimental Section and Supporting Information for details). As expected, DFT predicted a $|\Delta d|$ for the iron–nitrogen distances in **Q3** of 21.2 pm (d_{HS}(Fe–N) = 220.4 pm; d_{LS}(Fe–N) = 199.2 pm) and much smaller C1···Fe1 distances for the low-spin complex (d_{LS}(C1···Fe1) = 304.4 pm; d_{HS}(C1···Fe1) = 318.6 pm).[47] Since we are not using specialised basis sets,[48] we will not comment on the energetic differences between both spin states.

To shed some light on the different HS–LS transition temperatures of **3** observed in solution (≈213 K) and the solid-state (≈267 K) for solvent-free samples of **3**, and to get an idea of the influence of both THF solvent molecules and cooperative effects[49] in the solid-state, we inspected the crystal packing and the continuous temperature-dependence of the unit cell parameters more closely. On the molecular level, the changes induced by the spin transition bear some resemblance to a symmetrical breathing, as mentioned above. As can be seen from the parameters in Table 3, whereas the cell volume decreases significantly at low temperature, the lattice parameters do not change uniformly. Thus, while b and c are considerably smaller at low temperatures, the value for a becomes larger upon cooling a single crystal of **3**·2THF from 278 to 178 K. This can be explained by taking a closer look at the packing of the complexes in the crystal, which form a columnar structure in the a direction (Figure 9). The zwitterionic iron complexes within the individual chains adopt a tilted arrangement to each other with close contacts (closest H···H separation: 272 pm). The

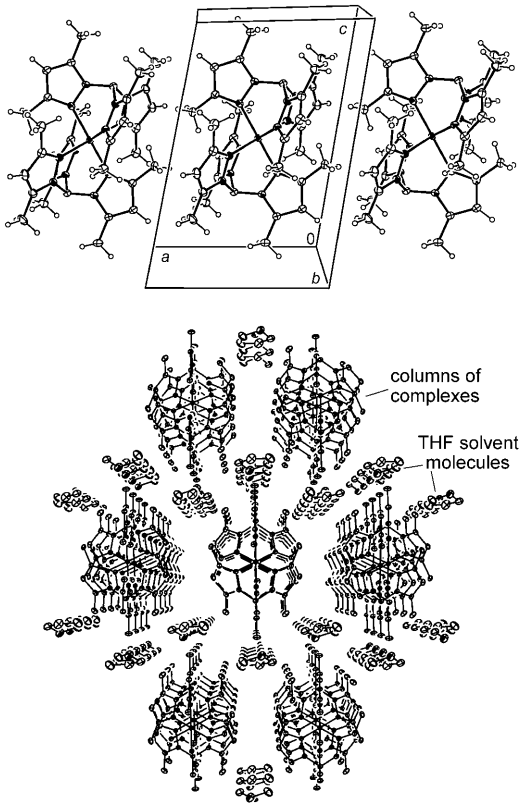

Figure 9. Different views of the crystal packing of **3**·2THF in the solid state (picture of the unit cell (top) without THF solvent molecules).

THF solvent molecules are embedded in between the hexagonally arranged chains of complexes.

As mentioned above, the Fe–N distances become considerably shorter upon changing the spin state from HS to LS. This shortening within the individual complexes has, in turn, structural consequences within the columns of complexes. As an inherent structural response of the ^{Me}Tpmd ligand, the pz rings are slightly rotated with respect to each other, which means that the CH_3 groups in the 5-position and the CH_{pz} moiety in the 4-position move towards neighbouring molecules in the *a* and *b* directions, thus causing intermolecular steric interactions. These interactions are obviously much more pronounced within the columns of complexes (*a*) than in between (*b*). Furthermore, the complexes are "compressed" in the *c* direction at low temperatures (much shorter Fe···C distances), hence we observe an elongation of the lengths of the columns of complexes (the value of *a* is larger at low *T*) while the distances between them (*b* and *c*) become shorter at low temperatures.[32]

To gain a suitable entry point for interpreting the influence exerted by incorporated solvent molecules on the HS–LS transition temperature in detail, we recorded the unit cell parameters of **3**·2THF between 283 and 163 K. As can be seen from Figure 10, we were able to detect the expected abrupt changes in the unit cell parameters at a temperature of around 193 K. The above-mentioned lengthening in the *a* direction is particularly significant at this temperature.

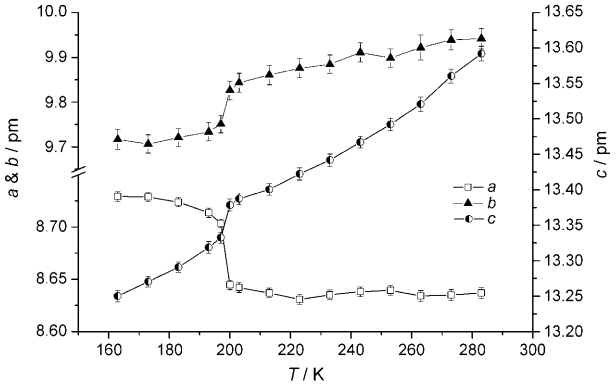

Figure 10. Temperature-dependence of the unit cell parameters *a*, *b* and *c* of **3**·2THF between 283 and 163 K ($\Delta T = 10$ K and smaller in the region of most interest at a temperature of around 200 K)

These findings clearly show that the HS–LS transition temperature is lowered by around 70 K with respect to the SQUID results for solvent-free samples of **3** ($T = 267$ K) and that incorporated solvent molecules can profoundly influence the electronic properties. Sensitive characteristics like the spin-transition behaviour can only be interpreted in more detail by using complementary techniques.

Electrochemistry: Since redox-active transition metal atoms are present in both complexes, the electrochemical properties of **3** and **4** were investigated by cyclic voltammetry (CV) in THF. This was of particular interest since combined electrochemical/HS–LS transition events may be anticipated for these complexes.

As can be seen from the DFT-calculated MO diagram (see above), the fact that the ^{Me}Tpmd ligand might show "non-innocent ligand"[50] behaviour, owing to the energetic destabilisation of the carbanions has to be kept in mind. Since the carbanionic moieties are very close in energy to the metal-centred frontier orbitals, redox processes, which are commonly assumed to be metal-centred [Eqn. (5)], may alternatively originate from the carbanionic ligand backbone [Eqn. (6)].

$$[M^{II}(^{Me}Tpmd)_2] \rightleftharpoons [M^{III}(^{Me}Tpmd)_2] + e^- \quad (5)$$

$$[M^{II}(^{Me}Tpmd)_2] \rightleftharpoons [M^{II}(^{Me}Tpmd)(^{Me}Tpmd)^{\bullet}] + e^- \quad (6)$$

To exclude the possibility of these types of process, we examined the redox behaviour of the related zwitterionic magnesium complex $[Mg(^{Me}Tpmd)_2]$[18] prior to our CV studies on **3** and **4**. $[Mg(^{Me}Tpmd)_2]$ contains the redox-inactive magnesium(II) cation and DFT predicts a *C*-centred HOMO. Indeed, we were only able to detect a broad and not well-defined irreversible oxidation process. We assume that this oxidation process is ligand-centred and produces the radical $[^{Me}Tpmd]^{\bullet}$ coordinated to Mg^{II}. The resulting complex is not stable and decomposes via an irreversible redox process. The same conclusions were recently drawn by Kinoshita et al. for a related, though intramolecularly coordinating,

ambidentate ligand and its copper and zinc complexes.[1,51] Based on our experimental and DFT studies, we have therefore assumed the metal-centred redox processes shown in Equation (5) for **3** and **4** during our discussion of the electrochemical findings, and present the first experimental evidence.

The cobalt complex **4** shows an irreversible electrochemical reduction between −2.55 and −2.65 V at room temperature (vs. the Fc/Fc^+ (Fc: ferrocene) couple with a potential of 0.352 V versus Ag/AgCl).[52] More interestingly, the irreversible oxidation that occurs between −0.25 and −0.10 V generates an oxidized species which is then re-reduced at around −1.10 V; a value 800 to 1000 mV more cathodically shifted. As can be seen from Figure 11, this latter reduction

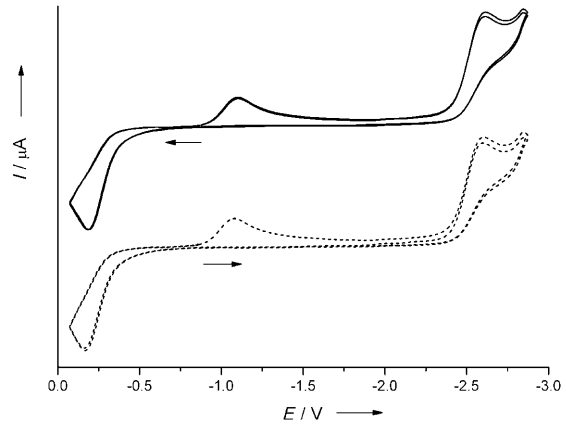

Figure 11. Cyclic voltammetry of **4** at room temperature in THF vs. Fc/Fc^+. Scan rate: 100 mV s^{-1}; Pt/[nBu$_4$N][PF$_6$]/Ag. The arrows indicate two principal sequences (two cycles each); solid line (top): oxidation–reduction run; dotted line (bottom): reduction–oxidation run.

wave can only be detected if the oxidized species is electrochemically generated first by an initial sweep in the positive direction (top trace of Figure 11 or second cycle in the bottom trace). This suggests that both half-wave potentials are undoubtedly related and that either an EC mechanism[53] or a combined electron-transfer and spin-transition is operating.[54–56] Indeed, comparably large differences between the anodic and cathodic peak potentials ($\Delta\phi_p$) of up to 1 V have been reported previously for some combined electron-transfer and spin-exchange cobalt(II/III) processes, although the peaks were sometimes broad and not well-defined.[54,57] As pointed out recently by Evans et al., the redox reactions and structural changes of many octahedral metal complexes can be classified as concerted.[58] The structural changes are governed by a change of the metal–ligand bond lengths (in this case MN_6 "breathing" mode), with no detectable intermediates being formed. When the energy term for the structural changes is large, which equates to a large reorganisation energy term, the transition state will be high as a result of Franck–Condon restrictions. A small electrochemical transfer rate constant is usually detected in such cases. Schultz et al. have performed extensive studies on coupled electron-transfer and spin-transition systems using electrochemical square schemes and thermodynamic parameters derived from simulations of CV experiments.[54–56]

To shed further light on the redox properties of **4**, we performed some preliminary preparative reactions. Unfortunately, only insoluble salts were obtained upon treating a solution of **4** in THF with one equivalent of the ferrocenium salt [Fc][PF$_6$]. Although the dark blue-green colour of $[Fc]^+$ gradually disappeared after stirring the reaction mixture for 12 h, and ferrocene could be sublimed in vacuo after evaporation of the solvent, we were not able to obtain unambiguous ^{1}H NMR spectroscopic data, owing to the low solubility of the salt [Co(^{Me}Tpmd)$_2$][PF$_6$] (**5**). A nicely soluble product could only be obtained by using weakly coordinating anions such as [Al{OC(CF$_3$)$_3$}$_4$]$^-$ ([PF]$^-$)[59] in NMR tube scale reactions. As expected, the resonances of a symmetrical, diamagnetic Co^{III} complex, with chemical shifts of $\delta = 1.02$, 2.74 (CH_3) and 6.03 ppm (CH_{pz}), could be detected. Discussion of the precise characterisation and molecular structures of both the [PF]$^-$ salt of **5** and the synthetically valuable ferrocenium salt [Fc][PF] is beyond the scope of this work.[60] Suffice it to say that this preliminary experiment verifies the postulation of a combined electron-transfer and spin-transition process observed in the CV. As would be expected, the low-spin form of **5**, which has a nominal $(20a_{1g})^2$, $(31e_g)^4$ electron configuration, is more stable than its high-spin counterpart (HS-**5**; $(20a_{1g})^2$, $(31e_g)^2$, $(32e_g)^2$; Equation (7)). We are currently not able to comment on whether this process can be classified as concerted or coupled as studies in this respect are still in progress.

$$\text{HS-}[Co^{II}(^{Me}Tpmd)_2]\ (\mathbf{4}) \rightleftharpoons \text{LS-}[Co^{III}(^{Me}Tpmd)_2]^+\ (\mathbf{5}^+) + e^- \quad (7)$$

In contrast, the analogous iron(II) complex shows only one quasi-reversible[61b] oxidation wave centred at −0.32 V (vs. Fc/Fc^+; see Figure 12). Assuming a metal-centred redox process (see above), the iron(II) complex is comparatively easily reversibly oxidised to the corresponding Fe^{III} complex. The oxidation potential is shifted by about 1 V to more negative values with respect to the analogous dicationic bis-

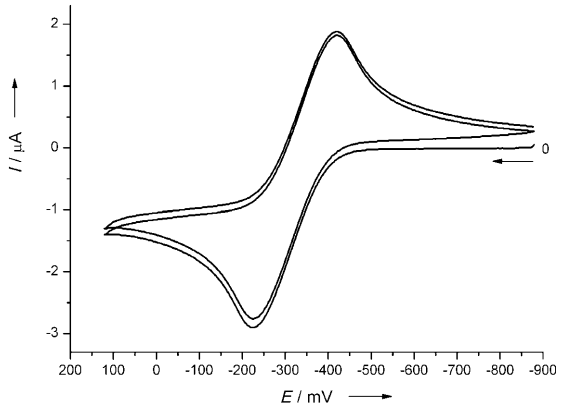

Figure 12. Cyclic voltammetry of **3** at room temperature in THF vs. Fc/Fc^+. Scan rate: 100 mV s^{-1}; Pt/[nBu$_4$N][PF$_6$]/Ag.

Table 4. Selected redox potentials $E^0_{1/2}(Fe^{II}/Fe^{III})$ in V vs. the ferrocene/ferrocenium couple (Fc/Fc^+) for closely related iron "sandwich" complexes containing κ^3N-donor ligands.

Complex	$E^0_{1/2}(Fe^{II}/Fe^{III})$ [V vs. Fc/Fc^+]	Conditions	Ref.
$[Fe(^{Me}Tpmd)_2]$ (**3**)	−0.32	$TBAPF_6$/THF	This work
$[Fe(^{Me}Tpm)_2]^{2+}$	+0.70	$TBAPF_6/CH_3CN$	[55]
$[Fe(Tpm)_2]^{2+}$	+0.69	$TBAPF_6/CH_3CN$	[55]
$[Fe(pzTp)_2]$	−0.17	$TBAPF_6/1,2\text{-}Cl_2C_2H_4$	[56]
$[Fe(Tp)_2]$	−0.27	$TBAPF_6/1,2\text{-}Cl_2C_2H_4$	[56]
$[Fe(Tp^*)_2]$	−0.44	$TBAPF_6/1,2\text{-}Cl_2C_2H_4$	[56]

[tris(pyrazolyl)methane]iron(II) complexes $[Fe(HC\{3,5\text{-}Me_2pz\}_3)_2]^{2+}$ ($E^0_{1/2}=0.70$ V) and $[Fe(HC\{pz\}_3)_2]^{2+}$ ($E^0_{1/2}=0.69$ V) recently published by Schultz.[55] Oxidation of the neutral bis[poly(pyrazolyl)borate]iron(II) complexes occurs in a similar region (see Table 4).[56]

Generally, as the stability of an Fe^{III} complex increases it becomes more difficult to reduce. A comparison of the Cp^- and Cp^{*-} anions clearly shows that the latter is more electron donating, mainly as a consequence of the methyl substituents. This is nicely reflected by the Fe^{II}/Fe^{III} redox potentials of the ferrocene complexes Cp_2Fe ($E^0_{1/2}=0.00$ V) and Cp^*_2Fe ($E^0_{1/2}=-0.59$ V), with a much more negative value being found for the bis(pentamethylcyclopentadienyl) complex. Consequently, $[Cp^*_2Fe]^+$ is considerably stabilized and more difficult to reduce. The redox potential can be shifted substantially to more positive values by employing more electron-withdrawing Cp ligands ($[FeCp(C_5H_4COMe)]$: $E^0_{1/2}=+0.27$ V; $[Fe(C_5H_4COMe)_2]$: $E^0_{1/2}=+0.49$ V).[62] Hence, in light of the negative potential of **3** ($E^0_{1/2}=-0.32$ V), the hexamethyl-substituted ^{Me}Tpmd ligand[63] can be classified in terms of electron-donating properties as being similar to Trofimenko's hexamethyl-substituted Tp* ligand (see Table 4).[64] Furthermore, these electrochemical results confirm our earlier assumption that the metal cations experience more or less the same ligand environment in Tp^R and ^{R}Tpmd complexes. Owing to the intrinsic single negative charge, both differ from the neutral ^{R}Tpm analogues, which means that sandwich-type complexes of divalent metal cations with ^{R}Tpm ligands are dicationic, whereas those with Tp^R and ^{R}Tpmd ligands are neutral.

As stated by Schultz et al.,[65] iron(III) complexes of poly(pyrazolyl)borate ligands exhibit magnetic moments in DMSO solutions consistent with LS-Fe^{III} complexes, as previously found by O'Hare for $[Fe(Tp^*)_2]^+$ in the solid state.[66] The corresponding iron(II) complex $[Fe(Tp^*)_2]$ has been shown to be high-spin in THF solution between 220 and 320 K. Electrochemical studies on $[Fe(Tp^*)_2]$ in 1:1 acetone/THF have shown that a coupled electron transfer and spin exchange takes place upon oxidation.[65] Although we have performed some initial oxidation reactions (see below), we cannot currently exclude such a combined process, in other words HS-Fe^{II} ⇌ LS-Fe^{III} for the oxidation of **3** at room temperature.

The difference in the peak potentials ($\Delta\phi_p$) observed for the quasi-reversible redox wave of **3** at room temperature is similar to that observed for $[Fe(Tp^*)_2]$.[65] To shed some light on the influence of the experimentally observed HS–LS solution equilibrium of **3** on its redox properties, we measured the temperature-dependence of $E^0_{1/2}$. The ^{1}H NMR spectroscopic studies discussed above suggested the onset of the spin equilibrium at a temperature of around 253 K and possibly an influence on the position of $E^0_{1/2}$ and its overall shape.[67] The cyclovoltammograms measured upon sequentially lowering the temperature ($\Delta T=10$ K) of our electrochemical cell by using a cooling jacket connected to an external cryostat system are shown in Figure 13.

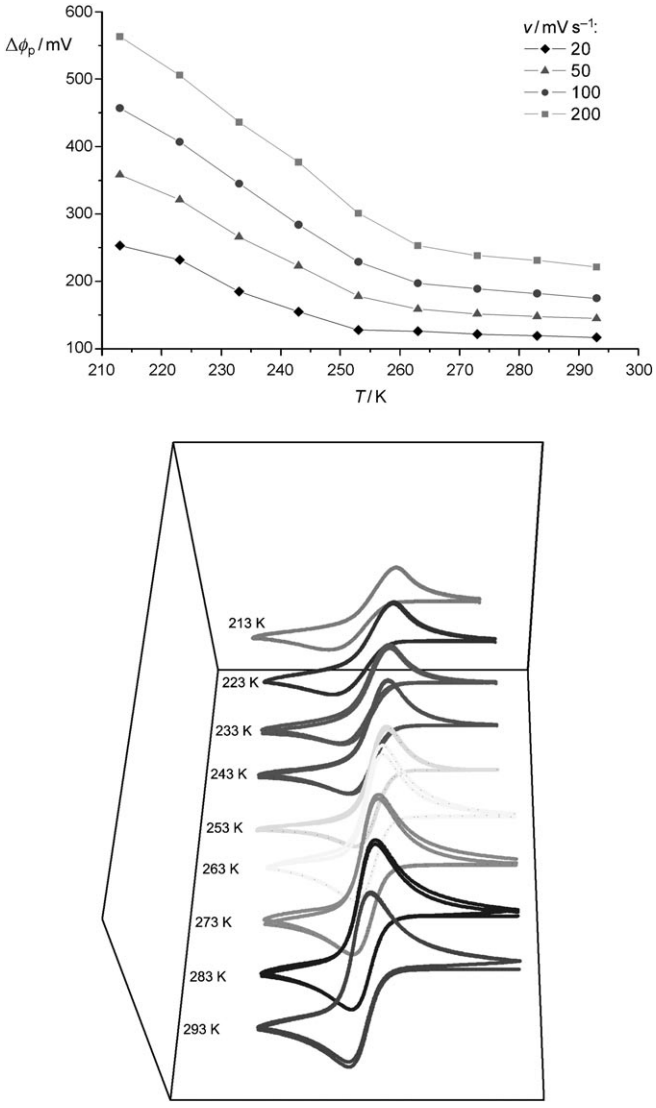

Figure 13. Temperature-dependent cyclic voltammetry of **3** (bottom, $v=100$ mV s^{-1}); top: differences of the peak potentials $\Delta\phi_p=\phi_p{}^a-\phi_p{}^c$ as a function of temperature (293–213 K, $\Delta T=10$ K) and scan rate ($v=20$, 50, 100, 200 mV s^{-1}).

As can be seen from the stack plot (Figure 13, bottom), the shape of the quasi-reversible oxidation wave changes considerably upon lowering the temperature: some broadening of the cathodic (ϕ_p^c) and anodic (ϕ_p^a) peak potentials can be observed along with a slight shift of the potential to more positive values. Of particular note, however, is the difference $\Delta\phi_p$. We therefore examined the change of $\Delta\phi_p$ with T in more detail and found a clear non-linear dependence. For a scan rate, v, of 20 mV s^{-1} between 293 and 253 K (black diamonds in Figure 13, top) $\Delta\phi_p$ follows an essentially typical temperature-dependence. At temperatures below 253 K, however, a fairly abrupt and significant increase of $\Delta\phi_p$ is observed. The overall picture was confirmed by measurements at higher scan rates, although the onset of a marked change in $\Delta\phi_p$ was observed at slightly higher temperature. Owing to technical limitations,[68] we are currently not able to properly extract transfer rate constants and thermodynamic parameters.[69] Qualitatively, however, the experimental data can be explained by assuming a significant influence of the HS–LS transition at lower temperatures on the transfer rate constant. These electrochemical investigations suggest an onset of the spin equilibrium of **3** in solution at a temperature of around 253 K, which is in excellent agreement with the observations made by ^{1}H NMR spectroscopy.

As expected from its redox potential of −0.32 V (vs. Fc/Fc$^+$), and by analogy with the corresponding cobalt complex **4**, complex **3** should react readily with the ferrocenium salt [Fc][PF$_6$] to give the cationic complex [Fe(^{Me}Tpmd)$_2$][PF$_6$] (**6**). Indeed, a dark red, scarcely soluble powder was obtained upon treating a THF solution of **3** with one equivalent of [Fc][PF$_6$] (or [Fc][OTf]; Equation (8)).

$$[Fe(^{Me}Tpmd)_2]\ (\mathbf{3}) + [Fc][PF_6] \rightleftharpoons [Fe(^{Me}Tpmd)_2][PF_6]\ (\mathbf{6}) + [Fc] \quad (8)$$

After removing the solvent in vacuo the expected amount of ferrocene could be sublimed off. The ^{1}H NMR spectrum of **6** (slightly soluble in [D$_8$]THF) shows the signals already observed, owing to the presence of a negligible amount of a ferromagnetic by-product formed during the synthesis of **3** (see above). Interestingly, the paramagnetic cation **6** is apparently not symmetric in solution, as suggested by the presence of two different pyrazole resonances ($\delta(CH_{pz}) = 55.5$ and 46.1 ppm). Furthermore, the methyl substituents show one very broad resonance with a chemical shift of $\delta =$ 40.7 ppm as well as two rather sharp signals at $\delta = 19.3$ and 14.7 ppm. The relative ratios from the integration of the signals (approx. 1:1) suggest the presence of two different ^{Me}Tpmd ligands. The data are also consistent with a slow HS-**6** ⇌ LS-**6** equilibrium coincidently consisting of an approximate 1:1 mixture of the spin fractions at room temperature. The triflate analogue and the product of NMR tube scale reactions with the [PF]$^-$ salt,[60] however, showed the same resonances, with identical integrations, in the ^{1}H NMR spectrum. These data allow us to exclude a significant influence of the counter-anion on the structure of the cationic iron complexes, owing to ion-pairing effects. The "asymmetry" of the complex consisting of two sets of signals for two different ^{Me}Tpmd ligands cannot, however, be explained and remains the subject of speculation. EPR, SQUID and Mössbauer investigations, more detailed CV investigations, including simulations, as well as further preparative studies using weakly coordinating anions[59] are currently under way.

Conclusion

We have described a systematic preparative, spectroscopic and theoretical study of the syntheses, structures and electronic properties of zwitterionic iron(II) (**3**) and cobalt(II) (**4**) sandwich complexes [M(^{Me}Tpmd)$_2$] containing κ^3N-coordinated tris(pyrazolyl)methanide ligands (^{Me}Tpmd). These complexes are the first such homoleptic 3*d* transition metal species to feature two "naked", outward pointing pyramidal carbanions. The two representative examples show iron- and cobalt-centred HOMOs and LUMOs (SOMOs) with the destabilised carbanion orbitals in the energy region of the filled transition-metal-centred frontier orbitals. Various spectroscopic techniques, such as NMR, EPR, SQUID, Mössbauer, etc., have shown that both complexes adopt a high-spin (HS) configuration at room temperature in solution and in the solid state. A thermally induced HS–LS transition was observed for the iron(II) complex **3**. Two main trends have been observed as a result of complementary studies on the transition temperature of **3** using a variety of techniques: a) the HS–LS transition temperature in solution differs from that in the solid state, which b) depends strongly on the amount of solvent molecules in the crystal lattice. Although a comparable thermally induced HS–LS transition is not observed for the related cobalt(II) complex **4**, electrochemical studies have shown that **4** undergoes a HS-Co^{II} ⇌ LS–Co^{III} transition upon oxidation. The electrochemical findings have been confirmed by preliminary synthetic oxidation reactions on a preparative scale. Overall, it can be concluded that the anionic Tp^R and ^{R}Tpmd ligands have similar bonding properties and that the metal atoms experience more or less the same ligand environment. However, within the family of polydentate six-electron κ^3N-donors, only ^{R}Tpmd shows ambidentate characteristics and dual functionality, the organometallic and coordination chemistry of which is the current focus of interest in our group.

Experimental Section

General techniques: All manipulations were performed under an argon atmosphere using standard Schlenk techniques. Chemicals were purchased from Aldrich and used without further purification. HC(Me$_2$pz)$_3$ was prepared according to a literature method and further purified by vacuum sublimation.[70] The acetonitrile salts [Co(acn)$_6$][(OTf)$_2$][71] and [Fe(OTf)$_2$(acn)$_2$][72] were used as starting materials to prepare the dicationic precursor compounds **1** and **2**, respectively. All solvents (pentane, hexane, Et$_2$O, benzene, THF) were freshly distilled under argon from

sodium/benzophenone (THF, benzene), sodium-potassium alloy/benzophenone (diethyl ether) or sodium-potassium alloy/tetraglyme/benzophenone (pentane, hexane) prior to use. [D_8]THF and C_6D_6 were vacuum-transferred from potassium/benzophenone into thoroughly dried glassware equipped with Young teflon valves. Air-sensitive compounds were stored and weighed in a glove box (Braun MB150 G-I or Unilab system). Elemental analyses and mass spectroscopic analyses were carried out in our institution's technical laboratories.

Spectroscopic methods: IR spectra were measured using either the ATR (attenuated total reflection) technique or between NaCl plates (Nujol mull) with a Bruker Vertex 70 spectrometer in the range from 4000 to 400 cm^{-1} using a KBr beam-splitter.

Cyclic voltammetry measurements were performed with an EG&G potentiostat (PAR-model 263 A) in an electrochemical cell for air-sensitive compounds.[61] We used a freshly polished Pt disk working electrode, a Pt wire as counter electrode and an Ag wire as reference electrode ([nBu$_4$N][PF_6] (0.1 M) as electrolyte). Potentials were calibrated against the Fc/Fc$^+$ couple ($E^0_{1/2}$ = 0.352 V vs. Ag/AgCl).[52]

Solution NMR spectra were recorded with Bruker Avance instruments operating at ^{1}H Larmor frequencies of 400 and 500 MHz and are referenced according to IUPAC recommendations.[73] Chemical shifts are given relative to TMS for ^{13}C and ^{1}H and $CFCl_3$ for ^{19}F. Coupling constants, J, are given in Hertz as positive values regardless of their real individual signs. The carbanionic carbon atom is indicated as $C_{anionic}$ and pyrazolyl units as CH_{pz} or C_{pz} when not identified otherwise.

The CW EPR spectrum at S-band (4.026 GHz) was measured with a home-built instrument[74] equipped with a liquid helium cryostat from Oxford, Inc. The temperature was 20 K, with a microwave (mw) power of 10 mW, a modulation amplitude of 0.5 mT and a modulation frequency of 100 kHz. At X-band (9.378 GHz), the CW EPR spectrum was recorded with a Bruker Elexsys E580 instrument at 20 K using a mw power of 22 mW, a modulation amplitude of 0.3 mT and a modulation frequency of 100 kHz. Spin-lattice relaxation rates ($1/T_1$) were determined at X-band with a Bruker Elexsys E580 spectrometer (mw frequency: 9.7 GHz) equipped with a liquid helium cryostat from Oxford, Inc. The saturation recovery measurements were measured with the pulse sequence $[t_p-t\ ]^{25}-T-\pi/2-t-\pi-$echo. A burst of 25 pulses with a length of 32 ns separated by a time interval of 240 ns was used with the maximum available mw power (1 kW). The recovery curve was monitored by the primary echo sequence using mw pulses of length $t_{\pi/2}$ = 50 and t_π = 100 ns. The observer position corresponded to $g_\perp$. A long repetition time of 5 ms was used to avoid spin saturation effects.

The magnetic measurements were performed with a Quantum Design SQUID magnetometer MPMS-XL. This magnetometer works between 1.8 and 400 K for dc applied fields ranging from −7 to 7 T. Measurements were performed with thoroughly dried, polycrystalline samples. The sample bag for the measurement was prepared and sealed in a glove box and then stored in a Schlenk tube before putting it into the SQUID. The magnetic data were corrected for the sample holder and the diamagnetic contribution.

Mössbauer spectra were acquired with a conventional spectrometer incorporating an Oxford Instruments Mössbauer-Spectromag 4000 Cryostat, equipped with a ^{57}Co source (3.7 GBq) in a rhodium matrix in the constant-acceleration mode. Isomer shifts are given relative to α-Fe at 300 K. Spectra were fitted using the NORMOS Mössbauer Fitting Program.

Computational details: DFT calculations were performed with the program TURBOMOLE.[75] The geometries were optimized at the (RI)-BP86[76] level with the def2-TZVP basis sets.[77] Analytical frequency calculations[78] were performed at the BP86/def2-TZVP level, and all species except one (LS-**Q3**) represent true minima without imaginary frequencies on the respective potential-energy surface. Further details, such as the complete list of coordinates, frequency analyses and energies of the calculated species are available as Supporting Information.

Crystal structure determination: Crystals of **3**·2THF and **4** suitable for X-ray diffraction were obtained by crystallisation from a concentrated THF solution at 5 °C. To avoid decomposition during the measurement the single crystals were mounted in perfluoropolyalkyl ether oil on top of a glass fibre and then placed in the cold nitrogen stream of a low-temperature device so that the oil solidified. Data collection for the X-ray structure determinations was performed with a STOE STADI 4 diffractometer equipped with a CCD area detector, a graphite-monochromated $Mo_{K\alpha}$ (0.71073 Å) radiation source and a low-temperature device. The temperature-dependence of the unit cell parameters a, b and c of **3**·2THF between 283 and 163 K (see Figure 10) was determined on one single crystal at different temperatures using the same exposure times and around 220 reflections. All calculations were performed with SHELXTL (v6.12) and SHELXL-97.[80] The structures were solved by direct methods and successive interpretation of the difference Fourier maps, followed by full-matrix least-squares refinement (against F^2). The contribution of the hydrogen atoms, in their calculated positions, was included in the refinement using a riding model. Upon convergence, the final Fourier difference map of the X-ray structures showed no significant peaks. Crystallographic data, data collection and refinement details are summarised in Table 5. CCDC 713965 and 713966 contain the supplementary crystallographic data for this paper. These data can be obtained free of charge from the Cambridge Crystallographic Data Centre via www.ccdc.cam.ac.uk/data_request/cif.

Synthesis of [Fe(^{Me}Tpmd)$_2$] (3): A solution of [NaN(SiMe$_3$)$_2$] (961 μmol, 1.60 mL; 0.6 M in toluene) was added to a stirred suspension of [Fe{HC(3,5-Me$_2$pz)$_3$}$_2$][(OTf)$_2$] (457 mg, 481 μmol) in THF (40 mL). After stirring for 1 h the solvent was removed in vacuo and the residue extracted with toluene (40 mL) and then filtered (P4). The solution was concentrated and stored at 5 °C to give colourless crystals of **3**. Yield: 191 mg (61 %); m.p.(sealed tube under Ar): 215 °C (decomposition); elemental analysis (%) calcd. for $C_{32}H_{42}FeN_{12}$: C 59.07, H 6.51, N 25.83, Fe 8.58; found: C 59.17, H 6.00, N 25.69; ^{1}H NMR (400 MHz, [D_8]THF, 298 K): δ = 13.5 (s, br, $W_{1/2}\approx$120 Hz, 18H; 5-CH_3), 39.4 (s, v br, $W_{1/2}\approx$630 Hz, 18H; 3-CH_3), 50.0 ppm (s, br, $W_{1/2}\approx$130 Hz, 6H; 4-CH_{Pz}); EI-MS (70 eV): m/z (%): 650.1 (7) [(M)$^+$], 352.8 (100) [(Fe[^{Me}Tpmd])$^+$], 202.9 (39) [(C(Me$_2$pz)$_2$)$^+$], 95.9 (9) [(Me$_2$pz)$^+$], 71.9 (9) [(C$_4$H$_{10}$N)$^+$], 41.9 (24) [(C$_2$H$_4$N)$^+$]; IR (solid, ATR): $\tilde{\nu}$ = 2957 vw (sh), 2923 w, 1548 m, 1450 m (sh), 1417 s (sh), 1394 s, 1363 m (sh), 1308 w, 1278 w, 1260 w, 1209 w, 1151 w, 1104 w, 1040 s, 980 vw, 904 vw, 871 s, 813 w, 768 vs, 730 m, 708 w, 658 w, 638 w, 590 vw, 571 vw, 496 s, 472 m, 417 cm^{-1} vw.

Synthesis of [Co(^{Me}Tpmd)$_2$] (4): A solution of [NaN(SiMe$_3$)$_2$] in THF (1 M; 2.1 mL) was added to a suspension of [Co{HC(3,5-Me$_2$pz)$_3$}$_2$][OTf]$_2$ (1.00 g, 1.05 mmol) in THF (20 mL) at −20 °C and the mixture allowed to warm to room temperature. The solvent was then removed in vacuo and the residue extracted with CH_2Cl_2 (20 mL) and filtered (P4). The filtrate was taken to dryness to give **4** as pale-yellow needles upon recrystallisation from THF at 5 °C. Yield: 370 mg (54 %); m.p.(sealed tube under Ar): 217 °C (decomposition); elemental analysis (%) calcd. for $C_{32}H_{42}CoN_{12}$: C 58.79, H 6.47, N 25.71, Co 9.03; found: C 58.97, H 6.010, N 25.38; ^{1}H NMR (400 MHz, C_6D_6, 298 K): δ = −87.2 (s, 3-CH_3), 50.9 (s, 5-CH_3), 52.2 ppm (s, 4-CH_{Pz}); EI-MS (70 eV): m/z (%): 653.3 (66) [M^+], 356.2 (100) [(Co[^{Me}Tpmd])$^+$], 203.3 (6) [(C(Me$_2$pz)$_2$)$^+$], 72.1 (17) [(C$_4$H$_{10}$N)$^+$], 42.1 (49) [(C$_2$H$_4$N)$^+$]; IR (solid, ATR): $\tilde{\nu}$ = 2924 w (sh), 1550 m, 1451 m, 1418 m, 1398 s, 1259 m, 1211 w, 1152 w, 1108 w, 1041 m (sh), 871 m, 768 s, 729 m, 639 m, 498 m, 474 cm^{-1} m.

Synthesis of [Co(^{Me}Tpmd)$_2$][PF_6] (5): A solution of **4** (70 mg, 10.7 μmol) and [Fc][PF_6] (35 mg, 10.5 μmol) in THF (20 mL) was stirred for 16 h at room temp. The solvent was then removed in vacuo and the ferrocene formed removed by sublimation onto a water-cooled finger. The tan-coloured residue was dried in vacuo and found to be insoluble in various solvents. A detailed discussion of the precise characterisation and molecular structures of both the [PF]$^-$ salt of **5** and the synthetically valuable ferrocenium salt [Fc][PF] will be published elsewhere.[60]

Synthesis of [Fe(^{Me}Tpmd)$_2$][PF_6] (6): Complex **3** (248 mg, 381 μmol) and [Fc][PF_6] (126 mg, 381 μmol) were stirred in THF (40 mL) for 2 h. The solvent was then removed in vacuo and the ferrocene formed removed by sublimation onto a water-cooled finger. The residue was suspended in THF and filtered. The red precipitate was washed with THF and dried in vacuo. Yield: 253 mg (83 %). Owing to its low solubility, **6** was characterised by ^{1}H NMR spectroscopy only. ^{1}H NMR (400 MHz, [D_8]THF,

298 K): $\delta = 14.7$, 19.3 (2×s, br, 9H, 9H; 2×3,5-CH_3), 40.7 (s, v br, 18H; 3,5-CH_3), 55.5, 46.1 ppm (2×s, br, 3H, 3H; 4-CH_{Pz}).

Table 5. Crystallographic data

Compound	**4**	LS-**3**	HS-**3**
empirical formula	$C_{32}H_{42}CoN_{12}$	$C_{32}H_{42}FeN_{12}$·$2C_4H_8O$	$C_{32}H_{42}FeN_{12}$·$2C_4H_8O$
M	653.71	794.83	794.83
crystal system	triclinic	triclinic	triclinic
space group[a]	$P\bar{1}$ (no. 2)	$P\bar{1}$ (no. 2)	$P\bar{1}$ (no. 2)
a [pm]	865.8(2)	875.7(2)	866.7(2)
b [pm]	985.1(2)	967.4(2)	991.1(2)
c [pm]	1046.4(2)	1327.9(3)	1357.5(3)
α [°]	66.79(3)	109.62(3)	109.11(3)
β [°]	86.09(3)	98.66(3)	98.39(3)
γ [°]	81.50(3)	100.81(3)	99.81(3)
V [$\times 10^6$ pm^3]	811.1(3)	1012.7(5)	1059.8(5)
μ [mm^{-1}]	0.572	0.423	0.404
ρ_{calcd} [g cm^{-3}]	1.338	1.303	1.245
crystal dimensions [mm]	0.15×0.15×0.10	0.40×0.25×0.15	0.40×0.25×0.15
Z	1	1	1
T [K]	150	178	278
$2\theta_{max}$ [°]	52.74	63.20	63.54
reflns. measured	6136	7997	8708
reflns. unique	3242 (R_{int}=0.0512)	4407 (R_{int}=0.0686)	4675 (R_{int}=0.0559)
parameters/restraints	210/0	256/0	256/0
$R1$ [$I \geq 2\sigma(I)$]	0.0528	0.0634	0.0610
$wR2$ (all data)	0.1463	0.1838	0.1897
max./min. res. elec. dens. [$e \times 10^{-6}$ pm^{-3}]	0.445/−0.542	1.383/−0.708	0.494/−0.494

[a] Ref. [79].

Acknowledgements

This work was supported by the Deutsche Forschungsgemeinschaft (DFG), the Fonds der Chemischen Industrie and the Ministerium für Wissenschaft, Forschung und Kunst Baden-Württemberg. We thank Prof. Ingo Krossing for the donation of some reagents and Helga Berberich for the measurement of some NMR spectra.

[1] Review: I. Kuzu, I. Krummenacher, J. Meyer, F. Armbruster, F. Breher, *Dalton Trans.* **2008**, 5836.

[2] Selected review articles and cited references: a) A. K. Saxena, J. A. Maguire, N. S. Hosmane, *Chem. Rev.* **1997**, *97*, 2421; b) A. K. Saxena, N. S. Hosmane, *Chem. Rev.* **1993**, *93*, 1081; c) N. S. Hosmane, J. A. Maguire, *Organometallics* **2005**, *24*, 1356; d) R. N. Grimes, *Coord. Chem. Rev.* **2000**, *200*, 773; e) R. N. Grimes, *Chem. Rev.* **1992**, *92*, 251; f) *Advances in Boron Chemistry* (Ed.: W. Siebert), RSC, Cambridge, **1997**; g) Z. Xie, *Coord. Chem. Rev.* **2002**, *231*, 23.

[3] The similarities between the Cp^- and [7,8-*nido*-$C_2B_9H_{11}]^{2-}$ were first recognised by Hawthorne et al.: M. F. Hawthorne, D. C. Young, P. A. Wegner, *J. Am. Chem. Soc.* **1965**, *87*, 1818.

[4] Selected review articles and cited references: a) W. A. Nugent, B. L. Haymore, *Coord. Chem. Rev.* **1980**, *31*, 123; b) M. H. Chisholm, I. P. Rothwell in *Comprehensive Coordination Chemistry, Vol. 2* (Eds.: G. Wilkinson, R. D. Gillard, J. A. McCleverty), Pergamon, Oxford, **1987**, p. 161; c) W. A. Nugent, J. M. Mayer, *Metal-Ligand Multiple Bonds*, Wiley-Interscience, New York, **1988**; d) D. E. Wigley, *Prog. Inorg. Chem.* **1994**, *42*, 239; e) P. Mountford, *Chem. Commun.* **1997**, 2127; f) P. R. Sharp, *Dalton Trans.* **2000**, 2647; g) T. R. Cundari, *Chem. Rev.* **2000**, *100*, 807; h) L. H. Gade, P. Mountford, *Coord. Chem. Rev.* **2001**, *216*, 65; i) R. A. Eikey, M. M. Abu-Omar, *Coord. Chem. Rev.* **2003**, *243*, 83; j) R. R. Schrock, A. H. Hoveyda, *Angew. Chem.* **2003**, *115*, 4740; *Angew. Chem. Int. Ed.* **2003**, *42*, 4592; k) U. Radius, *Z. Anorg. Allg. Chem.* **2004**, *630*, 957; l) N. Hazari, P. Mountford, *Acc. Chem. Res.* **2005**, *38*, 839.

[5] M. J. Ferreira, A. M. Martins, *Coord. Chem. Rev.* **2006**, *250*, 118.

[6] a) K. Dehnicke, F. Weller, *Coord. Chem. Rev.* **1997**, *158*, 103; b) K. Dehnicke, J. Strähle, *Polyhedron* **1989**, *8*, 707; c) K. Dehnicke, M. Krieger, W. Massa, *Coord. Chem. Rev.* **1999**, *182*, 19; d) K. Dehnicke, *Z. Anorg. Allg. Chem.* **2003**, *629*, 828; e) K. Dehnicke, A. Greiner, *Angew. Chem.* **2003**, *115*, 1378; *Angew. Chem. Int. Ed.* **2003**, *42*, 1340.

[7] a) M. Tamm, S. Randoll, E. Herdtweck, N. Kleigrewe, G. Kehr, G. Erker, B. Rieger, *Dalton Trans.* **2006**, 459; b) M. Tamm, S. Randoll, T. Bannenberg, E. Herdtweck, *Chem. Commun.* **2004**, 876.

[8] a) S. Trofimenko, *Chem. Rev.* **1993**, *93*, 943; b) S. Trofimenko, *Scorpionates: The Coordination Chemistry of Polypyrazolylborate Ligands*, Imperial, London, **1999**; c) G. Parkin, *Adv. Inorg. Chem.* **1995**, *42*, 291; d) D. L. Reger, *Coord. Chem. Rev.* **1996**, *147*, 571; e) M. Etienne, *Coord. Chem. Rev.* **1996**, *156*, 201; f) C. Janiak, *Coord. Chem. Rev.* **1997**, *163*, 107.

[9] For a comparison of Tp and Cp ligands see: a) D. M. Tellers, S. J. Skoog, R. G. Bergman, T. B. Gunnoe, W. D. Harman, *Organometallics* **2000**, *19*, 2428; b) E. Rüba, W. Simanko, K. Mereiter, R. Schmid, K. Kirchner, *Inorg. Chem.* **2000**, *39*, 382; c) N. J. Beach, A. E. Williamson, G. J. Spivak, *J. Organomet. Chem.* **2005**, *690*, 4640.

[10] a) H. R. Bigmore, S. C. Lawrence, P. Mountford, C. S. Tredget, *Dalton Trans.* **2005**, 635; b) C. Pettinari, R. Pettinari, *Coord. Chem. Rev.* **2005**, *249*, 525.

[11] a) L. H. Gade, *Acc. Chem. Res.* **2002**, *35*, 575; b) L. H. Gade, *J. Organomet. Chem.* **2002**, *661*, 85; c) L. H. Gade, *Eur. J. Inorg. Chem.* **2002**, 1257; d) L. H. Gade, *Chem. Commun.* **2000**, 173.

[12] For applications as a new class of highly productive, borate-free zwitterionic olefin polymerization catalysts see: a) M. Kranenbrug, G. H. J. Van Doremaele, B. Wang, M. A. Zuideveld, N. H. Friederichs, S. C. Lawrence, S. R. Dubberley, P. Mountford, WO 2005/123790, **2005**; see also Ref. [14b].

[13] a) P. K. Byers, N. Carr, F. G. A. Stone, *J. Chem. Soc. Dalton Trans.* **1990**, 3701; b) P. K. Byers, F. G. A. Stone, *J. Chem. Soc. Dalton Trans.* **1991**, 93.

[14] a) S. C. Lawrence, M. E. G. Skinner, J. C. Green, P. Mountford, *Chem. Commun.* **2001**, 705; b) H. R. Bigmore, S. R. Dubberley, M. Kranenburg, S. C. Lawrence, A. J. Sealey, J. D. Selby, M. A. Zuideveld, A. R. Cowley, P. Mountford, *Chem. Commun.* **2006**, 436.

[15] F. Breher, J. Grunenberg, S. C. Lawrence, P. Mountford, H. Rüegger, *Angew. Chem.* **2004**, *116*, 2575; *Angew. Chem. Int. Ed.* **2004**, *43*, 2521.

[16] I. Krummenacher, H. Rüegger, F. Breher, *Dalton Trans.* **2006**, 1073.

[17] Although the term "sandwich" complex is conventionally used to describe bis(cyclopentadienyl) complexes, it has also been used in the literature to describe different ligand systems.

[18] H. R. Bigmore, J. Meyer, I. Krummenacher, H. Rüegger, E. Clot, P. Mountford, F. Breher, *Chem. Eur. J.* **2008**, *14*, 5918.

[19] a) M. Veith, *Chem. Rev.* **1990**, *90*, 3; b) F. Baier, Z. Fei, H. Gornitzka, A. Murso, S. Neufeld, M. Pfeiffer, I. Rüdenauer, A. Steiner, T. Stey, D. Stalke, *J. Organomet. Chem.* **2002**, *661*, 111; c) M. Veith, S. Weidner, K. Kunze, D. Käfer, J. Hans, V. Huch, *Coord. Chem. Rev.* **1994**, *137*, 297; d) L. Mahalakshmi, D. Stalke, *Struct. Bonding* **2002**, *103*, 85, edited by D. A. Atwood, H. W. Roesky; see also for instance e) T. Stey, D. Stalke, *Z. Anorg. Allg. Chem.* **2005**, *631*, 2931; f) I. Krummenacher, C. Oschwald, H. Rüegger, F. Breher, *Z. Anorg. Allg. Chem.* **2007**, *633*, 2354.

[20] a) P. Gütlich, Y. Garcia, H. A. Goodwin, *Chem. Soc. Rev.* **2000**, *29*, 419; b) J. A. Real, A. B. Gaspar, V. Niel, M. C. Muñoz, *Coord. Chem. Rev.* **2003**, *236*, 121; c) A. Bousseksou, G. Molnár, G. Matouzenko, *Eur. J. Inorg. Chem.* **2004**, 4353; d) A. B. Gaspar, V. Ksenofontov, M. Seredyuk, P. Gütlich, *Coord. Chem. Rev.* **2005**, *249*, 2661;

e) A. Bousseksou, G. Molnár, J. A. Real, K. Tanaka, *Coord. Chem. Rev.* **2007**, *251*, 1822.
[21] C. Janiak, T. G. Scharmann, J. C. Green, R. P. G. Parkin, M. J. Kolm, E. Riedel, W. Mickler, J. Elguero, R. M. Claramunt, D. Sanz, *Chem. Eur. J.* **1996**, *2*, 992.
[22] The carbon-centred donor orbitals $[\boldsymbol{C}(pz)_3]^-$ were found to be energetically much higher (more destabilised) than their isoelectronic nitrogen ($\boldsymbol{N}(pz)_3$) or phosphorous ($\boldsymbol{P}(pz)_3$) counterparts. This becomes clear by comparing the DFT-calculated orbital energies of backbone-centred donor orbitals in homologous series. F. Breher, unpublished results; see also ref. [1].
[23] The analogous *P*- or *N*-donor ligands are much more energetically lowered (up to HOMO-11), which is in line with the observations made recently by Johnson et al. for multidentate *P*-based ligand sets: a) H. Han, M. Elsmaili, S. A. Johnson, *Inorg. Chem.* **2006**, *45*, 7435; b) R. Raturi, J. Lefebvre, D. B. Leznoff, B. R. McGarvey, S. A. Johnson, *Chem. Eur. J.* **2008**, *14*, 721.
[24] a) F. A. Walker, *Coord. Chem. Rev.* **1999**, *185–186*, 471; b) F. A. Walker, *Inorg. Chem.* **2003**, *42*, 4526; c) F. A. Walker, *Chem. Rev.* **2004**, *104*, 589.
[25] For a comparable behaviour of an iron(II) complex in solution see: D. W. Blakesley, S. C. Payne, K. S. Hagen, *Inorg. Chem.* **2000**, *39*, 1979.
[26] J. P. Jesson, S. Trofimenko, D. R. Eaton, *J. Am. Chem. Soc.* **1967**, *89*, 3158.
[27] D. L. Reger, C. A. Little, A. L. Rheingold, M. Lam, L. M. Liable-Sands, B. Rhagitan, T. Concolino, A. Mohan, G. J. Long, V. Briois, F. Grandjean, *Inorg. Chem.* **2001**, *40*, 1508.
[28] The electron configuration is given for the idealised D_{3d} symmetry (here and in the following).
[29] ($|\Delta\delta_{3,5}|$=difference between the chemical shifts of the methyl protons in the 3- and the 5-position.
[30] See for instance ref. [25].
[31] N. V. Shokhirev, F. A. Walker, TDFwg program: http://www.shokhirev.com/nikolai/programs/prgsciedu.html.
[32] P. Gütlich, A. Hauser, H. Spiering, *Angew. Chem.* **1994**, *106*, 2109; *Angew. Chem. Int. Ed. Engl.* **1994**, *33*, 2024.
[33] a) G. J. Long, B. B. Hutchinson, *Inorg. Chem.* **1987**, *26*, 608; b) S. Calogero, G. G. Lobbia, P. Cecchi, G. Valle, J. Friedl, *Polyhedron* **1994**, *13*, 87; c) D. L. Reger, C. A. Little, A. L. Rheingold, M. Lam, L. M. Liable-Sands, B. Rhagitan, A. Mohan, G. J. Long, V. Briois, F. Grandjean, *Inorg. Chem.* **2001**, *40*, 1508; d) D. L. Reger, C. A. Little, M. D. Smith, A. L. Rheingold, K. C. Lam, T. L. Concolino, G. J. Long, R. P. Hermann, F. Grandjean, *Eur. J. Inorg. Chem.* **2002**, 1190.
[34] See for example: a) C. Rajadurai, Z. Qu, O. Fuhr, B. Gopalan, R. Kruk, M. Ghafari, M. Ruben, *Dalton Trans.* **2007**, 3531; b) A. Galet, M. C. Muñoz, J. A. Real, *Chem. Commun.* **2006**, 4321; c) V. Niel, A. L. Thompson, M. C. Muñoz, A. Galet, A. E. Goeta, J. A. Real, *Angew. Chem.* **2003**, *115*, 3890; *Angew. Chem. Int. Ed.* **2003**, *42*, 3760; d) Y. Garcia, P. J. van Koningsbruggen, R. Lapouyade, L. Fournés, L. Rabardel, O. Kahn, V. Ksenofontov, G. Levchenko, P. Gütlich, *Chem. Mater.* **1998**, *10*, 2426; e) M. Hostettler, K. W. Törnroos, D. Chernyshov, B. Vangdal, N. B. Bürgi, *Angew. Chem.* **2004**, *116*, 4689; *Angew. Chem. Int. Ed.* **2004**, *43*, 4589; f) S. M. Neville, B. Moubaraki, K. S. Murray, C. J. Kepert, *Angew. Chem.* **2007**, *119*, 2105; *Angew. Chem. Int. Ed.* **2007**, *46*, 2059; g) G. J. Halder, C. J. Kepert, B. Moubaraki, K. S. Murray, J. D. Cashion, *Science* **2002**, *298*, 1762.
[35] A compilation of poly(pyrazolyl)borate complexes of iron(II) can be found in: D. L. Reger, J. R. Gardinier, J. D. Elgin, M. D. Smith, D. Hautot, G. J. Long, F. Grandjean, *Inorg. Chem.* **2006**, *45*, 8862.
[36] a) H. A. Goodwin in *Spin Crossover in Transition Metal Compounds II* (Eds.: P. Gütlich, H. A. Goodwin), Springer, Berlin, **2004**, p. 23; b) I. Krivokapic, M. Zerara, M. L. Daku, A. Vargas, C. Enachescu, C. Ambrus, P. Tregenna-Piggott, N. Amstutz, E. Krausz, A. Hauser, *Coord. Chem. Rev.* **2007**, *251*, 364.
[37] a) C. J. O'Connor, *Prog. Inorg. Chem.* **1982**, *29*, 203; b) O. Kahn, *Molecular Magnetism*, Wiley-VCH, Weinheim, **1993**.
[38] A. Abragram, B. Bleaney, *Electron Paramagnetic Resonance of Transition Ions*, Oxford University Press, Oxford, **1970**.
[39] J. P. Jesson, *J. Chem. Phys.* **1966**, *45*, 1049.
[40] W. K. Myers, E. N. Duesler, D. L. Tierney, *Inorg. Chem.* **2008**, *47*, 6701.
[41] a) R. Orbach, *Proc. R. Soc. London Ser. A* **1961**, *264*, 458; b) C. B. P. Finn, R. Orbach, W. P. Wolf, *Proc. Phys. Soc. London* **1961**, *77*, 261.
[42] ZFS is often represented by the symbol Δ, which in the case of $S = {}^3/_2$ is equal to $2(D^2+3E^2)^{1/2}$, in which D and E are parameters in the spin-Hamiltonian.
[43] a) M. W. Makinen, L. C. Kuo, M. B. Yim, G. B. Wells, J. M. Fukuyama, J. E. Kim, *J. Am. Chem. Soc.* **1985**, *107*, 5245; b) J. Krzystek, S. A. Zvyagin, A. Ozarowski, S. Trofimenko, J. Telser, *J. Magn. Reson.* **2006**, *178*, 174.
[44] a) D. L. Reger, C. A. Little, M. D. Smith, *Inorg. Chem.* **2002**, *41*, 4453; b) T. Astley, J. M. Gulbis, M. A. Hitchman, E. R. T. Tiekink, *J. Chem. Soc. Dalton Trans.* **1993**, 509; c) M. R. Churchill, K. Gold, C. E. Maw, *Inorg. Chem.* **1970**, *9*, 1597; d) C. Hannay, M. J. Hubin-Franskin, F. Grandjean, V. Briois, J. P. Itié, A. Polian, S. Trofimenko, G. J. Long, *Inorg. Chem.* **1997**, *36*, 5580; e) M. Lukasiewicz, Z. Ciunik, S Wolowiec, *Polyhedron* **2000**, *19*, 2119; f) T. Ruman, Z. Ciunik, A. Goclan, M. Lukasiewicz, S. Wolowiec, *Polyhedron* **2001**, *20*, 2965; g) M. Lukasiewicz, Z. Ciunik, T. Ruman, M. Skóra, S Wolowiec, *Polyhedron* **2001**, *20*, 237; h) T. Ruman, Z. Ciunik, S. Wolowiec, *Polyhedron* **2003**, *22*, 581.
[45] The steric repulsion of the lone pair of electrons at C1 and the Me substituents in the 5-position may inhibit an increase of the bite size to some extent.
[46] H. De Bari, M. Zimmer, *Inorg. Chem.* **2004**, *43*, 3344.
[47] Comparable distances were calculated for the D_{3d}-symmetric model compound $[Fe(^{H}Tpmd)_2]$ (**q3**), which contains the smaller ^{H}Tpmd ligand. See the Supporting Information for further details.
[48] a) M. Reiher, O. Salomon, B. A. Hess, *Theor. Chim. Acta* **2001**, *107*, 48; b) O. Salomon, M. Reiher, B. A. Hess, *J. Chem. Phys.* **2002**, *117*, 4729; c) H. Paulsen, A. X. Trautwein, *J. Phys. Chem. Solids* **2004**, *65*, 793; d) G. Lemercier, N. Bréfuel, S. Shova, J. A. Wolny, F. Dahan, M. Verelst, H. Paulsen, A. X. Trautwein, J.-P. Tuchagues, *Chem. Eur. J.* **2006**, *12*, 7421; e) H. Paulsen, L. Duelund, H. Winkler, H. Toftlund, A. X. Trautwein, *Inorg. Chem.* **2001**, *40*, 2201; f) H. Paulsen, L. Duelund, A. Zimmermann, F. Averseng, M. Gerdan, H. Winkler, H. Toftlund, A. X. Trautwein, *Monatsh. Chem.* **2003**, *134*, 295; g) H. Paulsen, J. A. Wolny, A. X. Trautwein, *Monatsh. Chem.* **2005**, *136*, 1107.
[49] Review on cooperative phenomena in iron(II) spin-crossover compounds: A. Hauser, J. Jeftiæ, H. Romstedt, R. Hinek, H. Spiering, *Coord. Chem. Rev.* **1999**, *190–192*, 471.
[50] See for instance: a) K. Ray, T. Petrenko, K. Wieghardt, F. Neese, *Dalton Trans.* **2007**, 1552; b) W. Kaim, G. K. Lahiri, Angew. Chem. **2007**, *119, 1808; Angew. Chem. Int. Ed.* **2007**, *46*, 1778; *Angew. Chem. Int. Ed.* **2007**, *46*, 1778; c) W. Kaim, *Coord. Chem. Rev.* **1987**, *76*, 187.
[51] a) R. Santo, R. Miyamoto, R. Tanaka, T. Nishioka, K. Sato, K. Toyota, M. Obata, S. Yano, I. Kinoshita, A. Ichimura, T. Takui, *Angew. Chem.* **2006**, *118*, 7773; *Angew. Chem. Int. Ed.* **2006**, *45*, 7611; b) K. Kitano, N. Kuwamura, R. Tanaka, R. Santo, T. Nishioka, A. Ichimura, I. Kinoshita, *Chem. Commun.* **2008**, 1314.
[52] N. G. Connelly, W. E. Geiger, *Chem. Rev.* **1996**, *96*, 877.
[53] C. H. Hamann, W. Vielstich, *Elektrochemie*, 4th ed., Wiley-VCH, Weinheim, **2005**.
[54] J. W. Turner, F. A. Schultz, *Coord. Chem. Rev.* **2001**, *219*, 81.
[55] a) J. R. Sheets, F. A. Schultz, *Polyhedron* **2004**, *23*, 1037; see also investigations in liquid SO_2 in b) P. R. Sharp, A. J. Bard, *Inorg. Chem.* **1983**, *22*, 2689.
[56] D. C. L. De Alwis, F. A. Schultz, *Inorg. Chem.* **2003**, *42*, 3616.
[57] For studies on combined electrochemical and HS–LS transition processes on Fe^{II}/Fe^{III} complexes see for instance: a) T. Ayers, S. Scott, J. Goins, N. Caylor, D. Hathcock, S. J. Slattery, D. L. Jameson, *Inorg. Chim. Acta* **2000**, *307*, 7; b) S. Singh, V. Mishra, J. Mukherjee, N. Seethalekshmi, R. Mukherjee, *Dalton Trans.* **2003**, 3392.

[58] a) N. A. Macías-Ruvalcaba, D. H. Evans, *Chem. Eur. J.* **2007**, *13*, 4386; b) D. H. Evans, *Chem. Rev.* **2008**, *108*, 2113.
[59] I. Krossing, I. Raabe, *Angew. Chem.* **2004**, *116*, 2116; *Angew. Chem. Int. Ed.* **2004**, *43*, 2066.
[60] I. Kuzu, I. Krummenacher, F. Breher, J. Slattery, I. Krossing, unpublished results.
[61] a) K. Hinkelmann, J. Heinze, H.-T. Schacht, J. S. Field, H. Vahrenkamp, *J. Am. Chem. Soc.* **1989**, *111*, 5078; b) J. Heinze, *Angew. Chem.* **1984**, *96*, 823; *Angew. Chem. Int. Ed. Engl.* **1984**, *23*, 831.
[62] F. Barrière in *Encyclopedia of Electrochemistry: Inorganic Electrochemistry, Vol. 7a* (Eds.: F. Scholz, C. J. Pickett), Wiley-VCH, Weinheim, **2006**, pp. 461–495.
[63] For a comparable effect of methyl substituents on Fe^{II}/Fe^{III} redox-potentials see for instance: A. K. Patra, M. Ray, R. Mukherjee, *Inorg. Chem.* **2000**, *39*, 652.
[64] For a comparison of the electronic properties of some tripodal ligands see for instance: C. A. Dodds, M.-A. Lehmann, J. F. Ojo, J. Reglinski, M. D. Spicer, *Inorg. Chem.* **2004**, *43*, 4927.
[65] J. W. Turner, F. A. Schultz, *J. Phys. Chem. B* **2002**, *106*, 2009.
[66] S. J. Mason, C. M. Hill, V. J. Murphy, D. O'Hare, D. J. Watkin, *J. Organomet. Chem.* **1995**, *485*, 165.
[67] See for instance: J. W. Turner, F. A. Schultz, *Inorg. Chem.* **2001**, *40*, 5296.
[68] To obtain an estimate for the rate constant k_0 we applied Equation (9) with $v = 0.020\ V\,s^{-1}$. The Λ values were approximated using tabulated data (See ref. [53], page 288) and an exponential curve fit. The diffusion coefficient D, although not known for **3**, was taken as a good estimate from our recent PGSE measurements (ref. [18]) on the zwitterionic magnesium complex $[Mg(^{Me}Tpmd)_2]$ ($D = 6.29 \times 10^{-10}\ m^2\,s^{-1}$).

$$k_0 = \Lambda \cdot \sqrt{D} \cdot \sqrt{\frac{n \cdot F}{R \cdot T}} \cdot \sqrt{v} \qquad (9)$$

As already expected from the qualitative description of the temperature-dependence of $\Delta\phi_p$, k_0 was found to be relatively constant between 293 and 253 K ($k_0 = 0.0015$–$0.0013\ cm\,s^{-1}$). Below this temperature range, the value of the rate constant drops considerably to $k_0 = 0.0009$ (243 K) and $0.0006\ cm\,s^{-1}$ (233 K). It is important to note that the rate constants obtained by this inexact and not simulated estimation are orders of magnitude lower than usually observed. We believe that uncompensated solution resistance (R_u) and other factors in our experimental setup have a strong influence. These values are therefore not discussed in detail and are just a relative comparison to obtain a general trend.
[69] a) See ref. [64]; b) J. K. Beattie, R. A. Binstead, R. J. West, *J. Am. Chem. Soc.* **1978**, *100*, 3044; c) Z. Zamponi, G. Gambini, P. Conti, G. G. Lobbia, R. Marassi, M. Berrettoni, P. Cecchi, *Polyhedron* **1995**, *14*, 1929.
[70] D. L. Reger, T. C. Grattan, K. J. Brown, C. A. Little, J. J. S. Lamba, A. L. Rheingold, R. D. Sommer, *J. Organomet. Chem.* **2000**, *607*, 120.
[71] R. A. Heintz, J. A. Smith, P. S. Szalay, A. Weisgerber, K. R. Dunbar in *Inorganic Synthesis, Vol. 33* (Ed.: D. Coucouvanis), Wiley, New York, **2002**, p. 75.
[72] K. S. Hagen, *Inorg. Chem.* **2000**, *39*, 5867.
[73] R. K. Harris, E. D. Becker, S. M. Cabral de Menezes, R. Goodfellow, P. Granger, *Pure Appl. Chem.* **2001**, *73*, 1795.
[74] M. Willer, J. Forrer, J. Keller, S. Van Doorslaer, A. Schweiger, R. Schuhmann, T. Weiland, *Rev. Sci. Instrum.* **2000**, *71*, 2807.
[75] a) TURBOMOLE Version 5.10, Turbomole GmbH, Karlsruhe, **2008**, see: http://www.turbomole.com; b) R. Ahlrichs, M. Bär, M. Häser, H. Horn, C. Kölmel, *Chem. Phys. Lett.* **1989**, *162*, 165; c) O. Treutler, R. Ahlrichs, *J. Chem. Phys.* **1995**, *102*, 346; d) M. Sierka, A. Hogekamp, R. Ahlrichs, *J. Chem. Phys.* **2003**, *118*, 9136; e) R. Ahlrichs, *Phys. Chem. Chem. Phys.* **2004**, *6*, 5119.
[76] a) J. C. Slater, *Phys. Rev.* **1951**, *81*, 385; b) S. H. Vosko, L. Wilk, M. Nusair, *Can. J. Phys.* **1980**, *58*, 1200; c) A. D. Becke, *Phys. Rev. A* **1988**, *38*, 3098; d) J. P. Perdew, *Phys. Rev. B* **1986**, *33*, 8822.
[77] Newly developed def2-TZVP-bases ("triple zeta valence augmented by polarization functions"): a) F. Weigend, R. Ahlrichs, *Phys. Chem. Chem. Phys.* **2005**, *7*, 3297; b) F. Weigend, *Phys. Chem. Chem. Phys.* **2006**, *8*, 1057.
[78] P. Deglmann, F. Furche, R. Ahlrichs, *Chem. Phys. Lett.* **2002**, *362*, 511.
[79] T. Hahn, *International Tables for Crystallography—Vol. A*, 5th ed., Kluwer Academic, Dordrecht, **2002**.
[80] a) SHELXTL v. 6.23, Bruker AXS Inst. Inc., Madison, WI, USA, **2000**; b) G. M. Sheldrick, *Acta Crystallogr. Sect. A* **2008**, *64*, 112.

Received: November 7, 2008
Published online: February 26, 2009

